GLOBAL IMAGING OF PROTON AND ELECTRON AURORAE IN THE FAR ULTRAVIOLET

S.B. MENDE[1], H.U. FREY[1], T.J. IMMEL[1], J.-C.GERARD[2], B. HUBERT[2] and S.A. FUSELIER[3]

[1]*Space Sciences Laboratory, University of California Berkeley, Berkeley, CA 94720, USA*
[2]*University of Liège, B-4000 Liège, Belgium*
[3]*Lockheed-Martin Advanced Technology Center, Palo Alto, CA, 94304, USA*

Abstract. The IMAGE spacecraft carries three FUV photon imagers, the Wideband Imaging Camera (WIC) and two channels, SI-12 and SI-13, of the Spectrographic Imager. These provide simultaneous global images, which can be interpreted in terms of the precipitating particle types (protons and electrons) and their energies. IMAGE FUV is the first space-borne global imager that can provide instantaneous global images of the proton precipitation. At times a bright auroral spot, rich in proton precipitation, is observed on the dayside, several degrees poleward of the auroral zone. The spot was identified as the footprint of the merging region of the cusp that is located on lobe field lines when IMF B_z was northward. This identification was based on compelling statistical evidence showing that the appearance and location of the spot is consistent with the IMF B_z and B_y directions. The intensity of the spot is well correlated with the solar wind dynamic pressure and it was found that the direct entry of solar wind particles could account for the intensity of the observed spot without the need for any additional acceleration. Another discovery was the observation of dayside sub-auroral proton arcs. These arcs were observed in the midday to afternoon MLT sector. Conjugate satellite observations showed that these arcs were generated by pure proton precipitation. Nightside auroras and their relationship to substorm phases were studied through single case studies and in a superimposed epoch analysis. It was found that generally there is substantial proton precipitation prior to substorms and the proton intensity only doubles at substorm onset while the electron auroral brightness increases on average by a factor of 5 and sometimes by as much as a factor of 10. Substorm onset occurs in the central region of the pre-existing proton precipitation. Assuming that nightside protons are precipitating from a quasi-stable ring current at its outer regions where the field lines are distorted by neutral sheet currents we can associate the onset location with this region of closed but distorted field lines relatively close to the earth. Our results also show that protons are present in the initial poleward substorm expansion however later they are over taken by the electrons. We also find that the intensity of the substorms as quantified by the intensity of the post onset electron precipitation is correlated with the intensity of the proton precipitation prior to the substorms, highlighting the role of the pre-existing near earth plasma in the production of the next substorm.

1. Introduction

Auroral emissions are created, either by energetic electrons, or protons through their interaction with atmospheric constituents, mainly N_2 and O. Most papers about spacecraft-based ultraviolet auroral observations interpret all emissions as being caused by electron precipitation measurements [e.g. Frank *et al.*, 1981; Frank and Craven, 1988; Anger *et al.*, 1987, Murphree *et al.*, 1994; Torr *et al.*, 1995;

Space Science Reviews **109:** 211–254, 2003.

Elphinstone *et al.*, 1996; Germany *et al.*, 1997]. However, energetic protons are very efficient in producing secondary electrons which in turn are capable of creating aurora indistinguishable from pure 'electron aurora' [Hubert *et al.*, 2001]. In general, the energy carried by the nightside energetic proton fluxes is relatively low compared to the energy of the electrons and the protons represent only a small contribution to the aurora. However at times and certain locations, protons may dominate and have to be taken into account [Frey *et al.*, 2001]. Furthermore protons, especially on the nightside, tend to be fairly energetic, with mean energies above 10 keV, and they are only minimally modulated by the field-aligned electric fields which have a fundamental influence on the electron aurora. Therefore, auroral protons are expected to be much better tracers of magnetospheric plasma populations than electrons. It is hoped that the global morphology of proton precipitation can be interpreted in terms of magnetospheric plasma regions.

Precipitating protons have been observed from spacecraft for many years. Such spacecraft-based global observations of proton aurora were restricted to statistical interpretations of the in situ particle measurements [e.g. Hardy *et al*., 1987, 1991]. Details of proton induced auroras, their global morphology, and their dynamics in response to interplanetary field, solar wind and substorm occurrences are still not as well understood. Although ground-based instruments were helpful in providing some missing information on such dynamics they are seriously constrained because proton auroras can only be observed in clear night conditions and then only by observing the relatively weak hydrogen Balmer emissions [Zwick and Shepherd, 1963; Eather, 1967]. These are the only emissions seen through the atmosphere that can be uniquely associated with proton precipitation. It is difficult to make observations of these weak emissions especially in the presence of strong and rapidly varying electron auroras during substorms [Mende and Eather, 1976].

On the dayside the observation of proton auroras from the ground is even more difficult because of the requirement of atmospheric darkness. These conditions can only be accomplished at certain geographic locations and only for relatively short periods around winter solstice. Techniques for the ground-based observation of low latitude proton auroras, such as the dayside detached arcs, are beyond the current state of the art.

The Far Ultraviolet (FUV) system on the IMAGE satellite is capable of making remote sensing global optical measurements of the aurora. The IMAGE FUV system consists of three simultaneously operating auroral cameras and a three-channel photometer for the measurement of the geocorona [Mende *et al*., 2000]. The Wideband Imaging Camera (WIC) observes the aurora in broad (140–170 nm) ultra violet band sensitive mainly to LBH N_2 and some NI lines. The SI-12, one of the two channels of the Spectrographic Imager (SI), images Doppler shifted Lyman – α to monitor the global proton precipitation. This instrument is an imaging monochromator, having a wavelength response resembling a picket fence that is virtually opaque at 1215.6 nm and high transmission at 121.8 nm and at 122.1 nm [Mende *et al.*, 2000]. Precipitating protons cascading into the atmosphere will un-

dergo charge exchange and produce spontaneous Doppler shifted Lyman – α whose wavelength is dependent on the line of sight velocity of the resulting hydrogen. The instrument is sensitive to emissions initiated by protons of energy >1 keV and it effectively suppresses Lyman alpha produced by the stationary geocoronal hydrogen. From the IMAGE orbit apogee (7 Re), it would be impossible to make proton auroral observations because of the presence of the intense (>10 kR) geocoronal Lyman alpha background unlike from low earth orbit [e.g. Ishimoto *et al.*, 1989]. Without the optical filtering of the SI-12 channel this background would appear as an impenetrable diffuse glow. There is a residual geocoronal contamination probably due to scattering within the instrument which is corrected by uniform background subtraction. A small amount of dayglow leak, most likely due to the 120.0 nitrogen emission, is also present, which is removed by dayglow correction in a manner similar to WIC or SI-13 dayglow correction.

The other SI channel, SI-13, images the atomic oxygen emission at 135.6 nm. The response of these instruments was validated by laboratory and by various in-flight calibrations. The most direct form of calibration included the observation of aurora during simultaneous spacecraft-based electron and ion flux measurements by the FAST spacecraft [Frey *et al.*, 2001; Gérard *et al.*, 2001].

In this paper we will review the IMAGE-FUV observations of the dayside cusp during times of $B_z > 0$ and enhanced solar wind dynamic pressure [Frey *et al.*, 2002]. A discussion including $B_z < 0$ is given by Fuselier *et al.* (2002a). The newly reported [Immel *et al.*, 2002] dayside detached aurora will be reviewed, and we will show that in most cases these arcs represent pure proton precipitation. Finally, an investigation of global proton and electron auroral morphology during substorms will be presented with a superimposed epoch analysis to derive the average properties of the proton and electron aurora during the substorms.

2. The IMAGE FUV measurements

Auroral emissions depend on the differential spectrum and flux of electrons and protons and on the composition of the atmosphere. A model calculation of the expected signal requires a full description of the particle spectrum for instance by in situ measurements from a low altitude satellite as done in [Frey *et al.*, 2001]. Measurements of the particles and particle energy fluxes are best accomplished by in situ detectors on satellites transiting the magnetospheric regions, however it is impossible to make instantaneous global scale measurements this way. Instead we use the imager data and infer equivalent particle fluxes that would produce the observed emissions. This equivalent particle flux is characterized by the total particle flux (particles/cm^2/s) and the mean energy (keV) of an assumed energy distribution (Gaussian, Maxwellian, or kappa-type). For completeness this approach would require the determination of 6 unknown parameters, the atmospheric density, composition (O/N_2 ratio), flux F and mean energies <E> of precipitating electrons

(e) and protons (p), respectively. In most instances the atmospheric density and the O/N_2 ratio is handled by using the MSIS model, however it is recognized that the composition can be highly variable in regions of intense auroral precipitation [Hecht *et al.*, 2000].

Detailed discussion of the IMAGE FUV calibrations and quantitative interpretations are given in an accompanying paper [Frey *et al.*, 2003]. Significant assumptions are needed for such interpretations. For example, most FUV imaging instruments flown on satellites including DE-1, Viking, POLAR UVI, VIS UV and IMAGE FUV imagers, had relatively wide wavelength bandwidth and they observed several auroral emission features simultaneously. The responsivity of these instruments, as expressed in output signal units per input Rayleighs depends on the spectral composition of the input photon flux. Without the precise knowledge of the input spectral distribution it is intrinsically impossible to derive input intensities from the measured signals. To evade this difficulty calibration of the responsivities for UV imagers is generally expressed as an equivalent responsivity for a single wavelength reference line source. However for realistic auroras the spectral composition depends on the fluxes of the different kind of precipitating particles, their energies, the mixing ratios of atmospheric constituents and the absorption of the atmosphere between the satellite and the source. For the quantitative interpretation of the instrument output signals in terms of precipitating particle energy flux in mW/m^2 goes even one step further by needing to model the auroral emission spectral composition and intensity from theoretical considerations and then folding the results into the measured (calibrated) responses of the instrument. All of these interpretation techniques make many assumptions. In this paper in most instances, where the interpretation of relative intensity changes are sufficient, the measurements were left in terms of corrected instrumental count rates rather than applying the complex assumptions needed for absolute interpretations. To obtain instrumental count rates a correction was applied to the raw counts to allow for the thermal variability of the IMAGE FUV detectors.The IMAGE satellite is in a highly elliptical orbit of $1000 \times 45\,600$ km altitude. The three sub instruments of the Far Ultra-Violet imager (FUV) observe the aurora for 5–10 seconds during every 2 minutes spin period [Mende *et al.*, 2000]. The major properties like fields of view, spatial resolution and spectral sensitivity were validated by in-flight calibrations with stars [Frey *et al.*, 2003]. The Wideband Imaging Camera (WIC) has a passband of 140–180 nm. It measures emissions from the N_2 LBH-band and atomic NI lines, with small contributions from the OI 135.6 nm line. The proton aurora imaging Spectrographic Imager channel (SI-12) instrument properties do not allow determination of the exact Doppler shift and energy of the emitting hydrogen atom. However, as was confirmed by theoretical modeling, it is mostly sensitive to proton precipitation in the energy range above 1 keV [Gèrard *et al.*, 2000, 2001]. The oxygen imaging Spectrographic Imager channel (SI-13) has a passband of 5 nm around the 135.6 nm oxygen (OI) emission. The measured signal is a combination of OI and some contribution from lines in the N_2 LBH emission band (20–50%

depending on electron energy). In summary the image FUV system produces 3 simultaneous images by the WIC, SI-12 and SI-13 instruments with an exposure time of 10, 5, and 5 seconds, respectively.

The WIC and SI-13 imagers observe emissions from atmospheric neutrals that are excited by secondary electrons produced by both precipitating electrons and protons. The SI-12 is sensitive only to the hydrogen emissions of the proton aurora. The generalized simplified description of the signal in the three FUV imaging channels can then be given as,

$$\mathrm{I(S12)} = \mathrm{F(p)} * \mathrm{b_{s12}}(< \mathrm{E_p} >) \quad (1)$$

$$\mathrm{I(WIC)} = \mathrm{F(p)} * \mathrm{b_{wic}}(< \mathrm{E_p} >) + \mathrm{F(e)} * \mathrm{a_{wic}}(< \mathrm{E_e} >) \quad (2)$$

$$\mathrm{I(S13)} = \mathrm{F(p)} * \mathrm{b_{s13}}(< \mathrm{E_p} >) + \mathrm{F(e)} * \mathrm{a_{s13}}(< \mathrm{E_e} >) \quad (3)$$

Where the output signals I (S12) and I (S13) are corrected photo electron counts, I (WIC) is CCD analog-to digital converter units, F(p) and F(e) are the proton and electron fluxes and $<E_p>$ and $<E_e>$ are the mean energy of protons and electrons, respectively. The a-s and b-s are the modeled quantities and they are a function of the mean energy of the electrons and protons and they include the instrument calibration factors. It is important to note that it is only the SI-12 signals, which represents 'pure' proton emission. Both the WIC and SI-13 respond to auroral emissions of atmospheric constituents, mainly nitrogen and oxygen, and the observed signal is a combination of the two types of primary precipitating particles. In this respect WIC and SI-13 are not different from the previously flown space borne FUV auroral cameras such as DE-1, Viking, Freja, POLAR UVI or POLAR VIS Earth cameras.

The measurements I(WIC), I(S12), and I(S13) provide three input parameters for calculating the global energy and flux distribution of auroral particles. The parameters a and b with the subscripts for every instrument are functions of the mean energy of electrons and protons and their value depends on the atmospheric models and the instrument parameters such as passband, gain etc. In quantitative observations our goal is to obtain the proton and electron fluxes F(p) and F(e) and the mean energy $<E_e>$ and $<E_p>$. Thus we have an intrinsically insoluble problem of four unknowns and three equations. Although proton energies are quite variable [e.g., Newell *et al.*, 1996], in order to proceed, we assume a mean energy for the protons of 2 keV for the dayside and 25 keV for the nightside. For all our simulations we will assume a Maxwellian distribution for electrons and a kappa distribution for protons [Gerard *et al.*, 2001; Hubert *et al.*, 2002]. A full description of the quantitative analysis of IMAGE-FUV observations is given in an accompanying paper [Frey *et al.*, 2003].

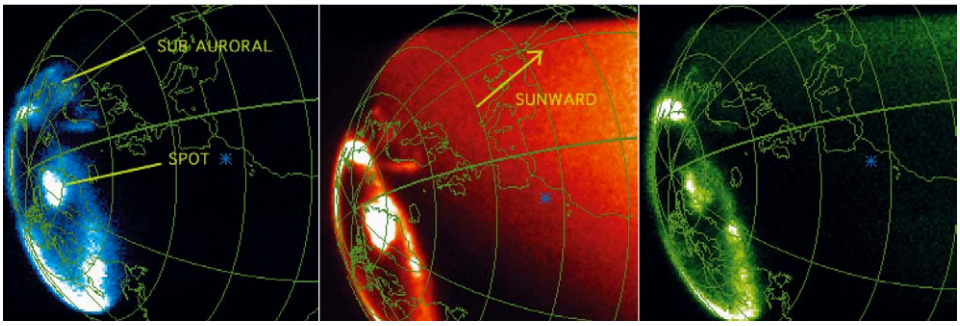

Figure 1. Intense cusp precipitation images taken by the IMAGE FUV instrument during a period of strongly northward IMF. The left image is taken by the SI-12 channel representing protons (blue) the middle by the WIC camera (red) produced by both electrons and protons and the right by the SI-13 channel. Intense SI-13 signal relative to the WIC signal represents soft precipitation.

3. Dayside IMAGE FUV observations

On several occasions the IMAGE-FUV images showed a curious configuration with a bright spot on the dayside well poleward of the auroral oval. An example of such a configuration is shown in Figure 1. In the figure we annotated the spot and the sub auroral arc feature on the SI-12 (blue) image. It was soon recognized that this high latitude spot configuration is usually seen when IMF B_z is positive [Frey *et al.*, 2002]. With the availability of simultaneous proton and electron aurora images we were able to examine the behavior of these cusp auroras and study their dependence on the direction of the IMF and the pressure of the solar wind.

It is interesting to note that a sub-auroral arc feature, subject of our later discussion, is also present. This is best seen in the SI-12 channel and it is located on the afternoon side in the image. In this case, this is a transient patch of precipitation, which is associated with the arrival of shocked solar wind at the magnetopause [Fuselier *et al.*, 2001; Zhang *et al.*, 2003].

3.1. Direct observation of the dayside cusp in conditions of B_z positive

Since its discovery by low-altitude polar orbiting satellites [Burch, 1968; Heikkila and Winningham, 1971; Frank, 1971; Russell *et al.*, 1971], the cusp has been known as the area where magnetosheath plasma could most easily access to lower altitude. Further statistical studies confirmed the localized nature of the cusp near local noon [e.g. Newell and Meng, 1994] and established our knowledge about the morphology, dynamics, particle and optical signatures of the cusp [e.g. Reiff *et al.*, 1977; Woch and Lundin, 1992; Sandholt, 1997; Dunlop *et al.*, 2000]. There are three major models describing the cusp morphology and dependence on external solar wind conditions, the MHD model, the turbulence/diffusive entry model, and the direct flowing entry model [see Yamauchi and Lundin, 2001 and references

therein]. These models describe many of the special cusp properties, but they are only partially successful in describing the low- and high-resolution observations, so that none of them describes everything (see Yamauchi and Lundin (2001) for a full discussion).

The magnetospheric cusp plays an important role as the region of most direct connection between the ionosphere and the interplanetary medium through reconnection [Smith and Lockwood, 1996]. Reconnection between magnetospheric and interplanetary magnetic field lines is likely to occur whenever their directions (or at least one strong component) are anti-parallel [Onsager and Fuselier, 1994; Fuselier *et al.*, 1997]. During southward IMF conditions, magnetic field lines on the low-latitude dayside magnetopause can connect to the solar wind magnetic field and become open. During northward IMF condition, reconnection can take place at the high latitude magnetopause. During intermediate conditions with small northward and dominating east-west components of the IMF, reconnection at the high- and the low-latitude region may occur simultaneously [Reiff and Burch, 1985].

Dayside auroral forms in the cusp region so far have mostly been classified from ground-based observations. During northward IMF conditions (clock angle $|\theta| < 45°$) bands of auroral emission dominate at high latitudes (78–79°, type 2 cusp aurora), during intermediate conditions ($|\theta| \sim$approx 45–90°) auroral bands are present at high and low ($< 75°$) latitudes, and during southward IMF ($90° > \theta > 270°$) the high-latitude aurora disappears, and only the low-latitude forms (type 1 cusp aurora) remain [Sandholt *et al.*, 1998]. These auroral forms show asymmetries depending on the IMF east-west B_y component, and are related to reconnection processes at either high- or low magnetopause latitudes [Oieroset *et al.*, 1997]. Ground based observations however were not able to resolve the global morphology of the cusp precipitation.

In a recent paper, Milan *et al.* [2000] described an event study of an interval of northward IMF, where they observed luminosity near local noon poleward of the dayside auroral oval with the UVI instrument on the Polar satellite. They interpreted this emission as the signature of high latitude reconnection and described its motion in response to IMF B_y changes in coordination with observations of the large-scale convection flow by the CUTLASS Finland HF radar.

The general properties of cusp auroras were studied by collecting 18 cases of a localized bright UV emission in the SI-12 images on the dayside during the time period from June 5 to November 26, 2000 (days of year 157-331). Figure 2 shows examples from four different days, when the localized feature or spot could be observed poleward of the dayside auroral oval location. The auroral configurations were especially pronounced in the images from the SI-12 channel representing proton auroras, because this channel has the least background from dayglow. However, after proper dayglow subtraction, similar features could be seen in the other FUV channels as well. Solar wind parameters for this study were determined using data from the WIND and Geotail spacecraft available through CDAWeb. All solar

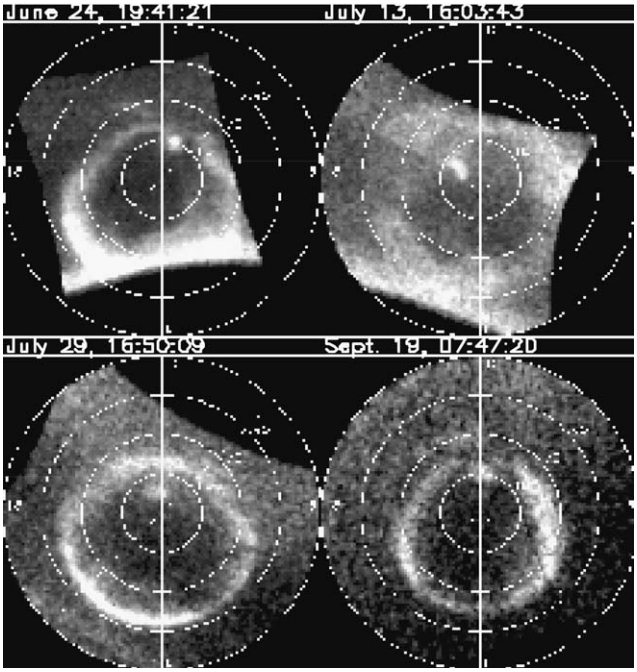

Figure 2. Examples of Cusp auroras during IMF $B_z > 0$ configuration.

wind properties were propagated to Earth using the instantaneous solar wind speed values.

For a statistical study we have collected events with the following selection criteria:
(1) a localized region of bright Doppler shifted Lyman alpha emission had to be present poleward of the dayside auroral oval. (2) the localized region had to be observable for at least 30 minutes. No selection criteria was used for magnetic activity. For the details of the study see Frey *et al.* (2002).

The propagated solar wind measurements were used to determine correlations between the proton precipitation location of the brightest spot, the spot intensity, and the solar wind magnetic field and plasma parameters. The relationship between the IMF GSM B_z value and the cusp location and Lyman alpha emission is given in Figure 3. Cusp observations were performed during periods of northward IMF and there does not seem to be a clear dependence of the latitude location of the spot and B_z (Figure 3a). This is in agreement for instance with Newell *et al.* [1989]. The intensity of the proton precipitation is strongly biased towards positive values of B_z (Figure 3b). However, there is no clear correlation between both quantities, as the correlation coefficient reaches only 0.41. There seem to be two subsets, one, which contains small SI-12 signals for positive and negative values of B_z, and one, which seems to show an increasing SI-12 signal with increasing positive B_z. However, both subsets could not be separated easily.

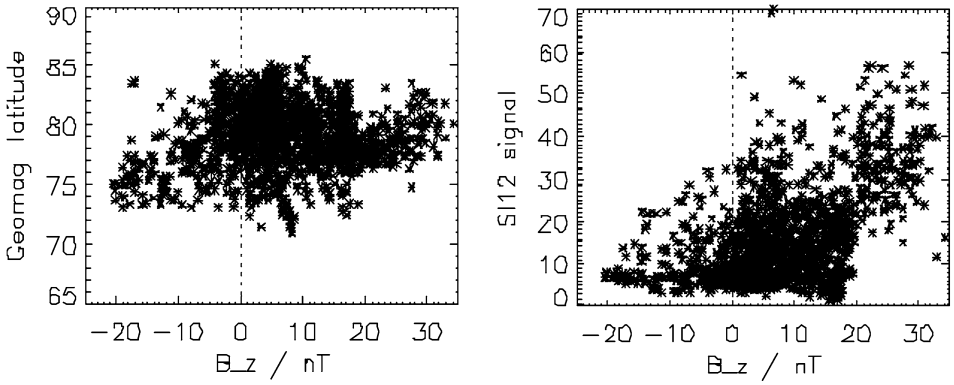

Figure 3. Scatter plot of cusp auroras. Geomagnetic latitude (left) and intensity (right) of auroral spots as a function of IMF B_z. The SI12 intensity is in photoelectron counts (35.6 counts per 1 mW/m^2 for modeled protons of 2 keV mean energy [Frey *et al.*, 2002]).

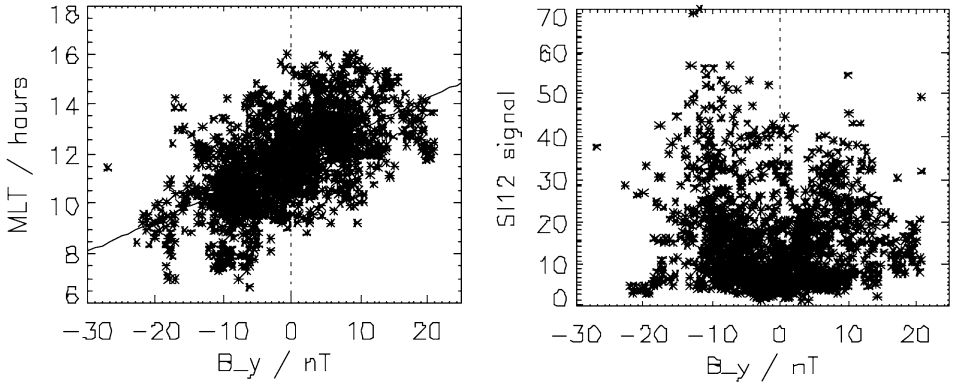

Figure 4. Scatter plot of cusp auroras. Magnetic local time (left) and intensity (right) of auroral spots as a function of IMF B_y. The SI12 intensity is in photoelectron counts same as Figure 3.

Figure 4 summarizes the dependence of the cusp magnetic local time location and proton precipitation on the value of IMF B_y. There is a clear correlation between the location and B_y with pre-noon location for negative B_y and post-noon location for positive B_y. The least squares fit of all the data provided a result as

$$\mathrm{MLT} = 11.8 + 0.127\mathrm{B_y}, \tag{4}$$

with B_y taken in nT, and MLT given in hours. The standard deviation of the fit is 0.003.

There is some indication that the response of the MLT location to IMF B_y changes is slower than for instance for emission changes in response to B_z changes. This finding is in agreement with Milan *et al.* (2000), who speculated about a dependence on the past history of the IMF. The locations of all cusp observations are given in Figure 5.

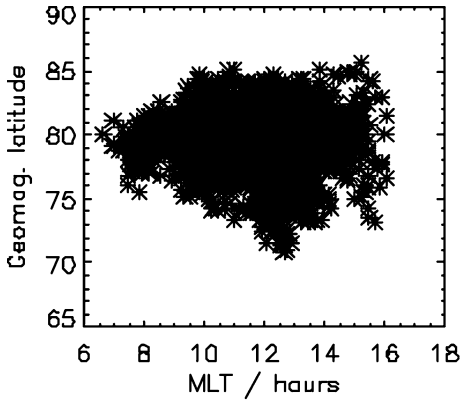

Figure 5. Geomagnetic latitude of auroral spots as a function of magnetic local time (MLT).

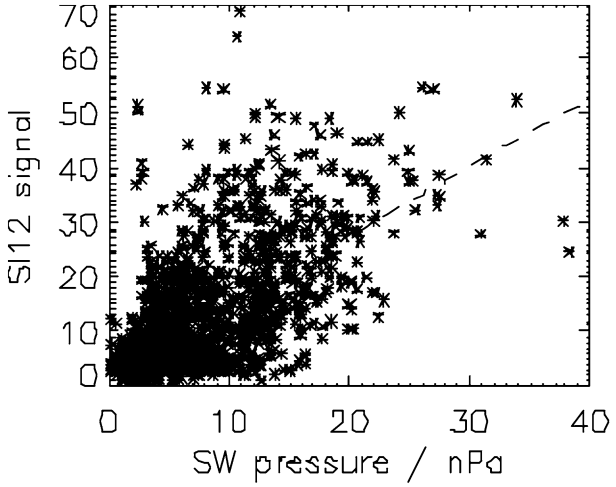

Figure 6. Intensity of auroral spots in the SI-12 channel as a function of solar wind pressure. The SI12 signal intensity is in photoelectron counts same as Figure 3.

Figure 6 summarizes the dependence of the cusp proton precipitation on the solar wind dynamic pressure. A much better correlation of 0.66 was determined for this relation between the cusp signal and the dynamic pressure compared to only 0.31 for the relation to the solar wind density. The least squares fit result is

$$\mathrm{SI12} = 2 + 1.2\mathrm{p_{dyn}} \tag{5}$$

with $\mathrm{p_{dyn}}$ in nPa, and SI12 given here as instrument counts. Assuming a mean energy of 2 keV for the precipitating protons, this would translate into a Lyman alpha intensity in Rayleigh of

$$\mathrm{I\ (Lyman\ \alpha)} = 500 + 300\mathrm{p_{dyn}} \tag{6}$$

The details of quantitative analysis process is described in the accompanying paper in this issue [Frey *et al.*, 2003].

The quantitative analysis of flux estimates as outlined above starts with a κ distribution of the protons with $\kappa = 3.5$ [Hubert *et al.*, 2001] and an assumed mean proton energy in the cusp of 2 keV. This is a reasonable assumption according to statistical investigations of the average proton energy in the cusp [Hardy *et al.*, 1989, 1991].

The SI-12 signal in the cusp is used to determine the proton flux which is needed for the proton correction of the WIC and SI-13 signals and the WIC to SI-13 ratio is then used to determine the mean energy of the precipitating electrons. This ratio is energy dependent because the SI-13 signal changes much more with energy of precipitating electrons than the WIC-signal, due to the deeper penetration of higher energy electrons into the atmosphere and the increased UV-absorption by molecular oxygen at the shorter wavelength. Therefore, the proton corrected WIC signal is finally used to determine the energy flux of electrons.

From the 1977 samples the proton energy fluxes are between 0.05 and 1 mW/m^2 for most of the observations with a mean value of 0.5 mW/m^2 while the standard deviation of the mean energy flux is 0.46. These are reasonable values compared to in-situ measurements by satellites like FAST or DMSP. After correcting for the proton contribution, the WIC/SI-13 ratio was used to calculate the mean energy of precipitating electrons. Most of the time this energy was below 1 keV (mean value 910 eV), but there are several single measurements with mean energies greater than 10 keV. Such mean energies are unreasonable for cusp precipitation. Here it has to be kept in mind, that the mean energy is estimated from the ratio of the WIC and SI-13 signals. Sometimes the SI-13 signal is very small (1-5 counts) riding on top of a dayglow signal of 20-40 counts. At such small count rates statistical fluctuations and a slightly incorrect dayglow subtraction may very easily change the ratio by 50%.

The calculated electron energy fluxes are around 1 mW/m^2 for most of the observations, which again is a reasonable flux in the cusp. Large excursions from this value coincide with periods of very high solar wind dynamic pressure. These deviations may indicate that the flux estimates may fail during periods of very large solar wind disturbances, when probably some of the simplifications outlined above may not be justified.

In general the calculated ratios of proton energy flux to electron energy flux show large fluctuations. However, here the uncertainty in the proton energy flux is not as large as the uncertainty in the electron energy flux because the SI-12 signal does not suffer from dayglow background. The median of the proton energy flux in the whole dataset is 0.26 and the mean is 0.30 mW/m^2. This means that for this complete dataset, generally, protons carry 26–30% of the energy flux that electrons do. This result is in very good agreement with a 27% estimate from model calculations for cusp precipitation using the statistical distribution of electron and proton precipitation [Hardy *et al.*, 1985, 1989] as input parameters [Hubert *et al.*, 2001].

The mean of the ratio of the proton produced SI-13 signal to the total signal in this whole data set is 11% but there are several cases where this ratio reaches 30%. The implication of this result is that ground based observations of auroral emissions from the cusp may have overestimated the electron energy flux if the analysis assumed that all emission was produced by electrons. This could especially be the case for red-line observations at 6300 nm, because this emission is as unstructured as the proton precipitation and can be misinterpreted as the signature of soft electron precipitation.

Equation (5) relates SI-12 counts to the solar wind dynamic pressure. After crossing the bow shock, the solar wind is slowed down with a simultaneous increase in density and temperature [e.g. Walker and Russell, 1995]. Therefore, the solar wind properties as measured by satellites will not be the same as properties for plasma entering the cusp. As a rough estimate however, we want to check if the solar wind in principle is able to provide the plasma, which could produce the cusp signature as seen by the proton imager.

During many of our events, we observe high solar wind density together with high bulk velocity. A solar wind bulk velocity of 619 km/s is equivalent to the speed of 2 keV protons. The solar wind density and flux required to produce the high dynamic pressures would provide a flux of protons, which is an order of magnitude more than would be required for the production of the proton aurora, if the solar wind could enter the cusp directly. Chang *et al.* (2002) discuss a single case of similar $B_z > 0$ cusp observations with IMAGE FUV and they claim that in that case particle acceleration was required to account for the intensity of the aurora. They also imply that some of the auroral flux changes seen are due to solar wind temperature variations.

Previous observations by Oieroset *et al.* (1997) showed particle data and discussed proton acceleration by magnetic tension forces after high-latitude reconnection. Enhanced auroral green-light emission was explained by electron acceleration at the magnetopause or at lower altitude. In another study, enhanced ionization in the cusp proper could be explained by either 1 keV electron or 3 keV proton precipitation and was considered as a result of additional acceleration in the cusp [Nilsson *et al.*, 1998]. Here we show that the solar wind provides enough energy and particle flux for our observations. Even after the interaction of the solar wind with the bow shock and in the magnetosheath, the high-energy tail of the Maxwellian solar wind proton distribution could account for our observations and an additional acceleration of the protons is not necessary to produce the observed cusp signatures in the optical emission from precipitating protons.

3.2. Subauroral proton precipitation. FUV Imaging of detached proton arcs

Auroral precipitation away from the normal auroral oval has been observed in visible wavelengths in ISIS-2 observations [Anger *et al.*, 1979; Moshupi *et al.*,

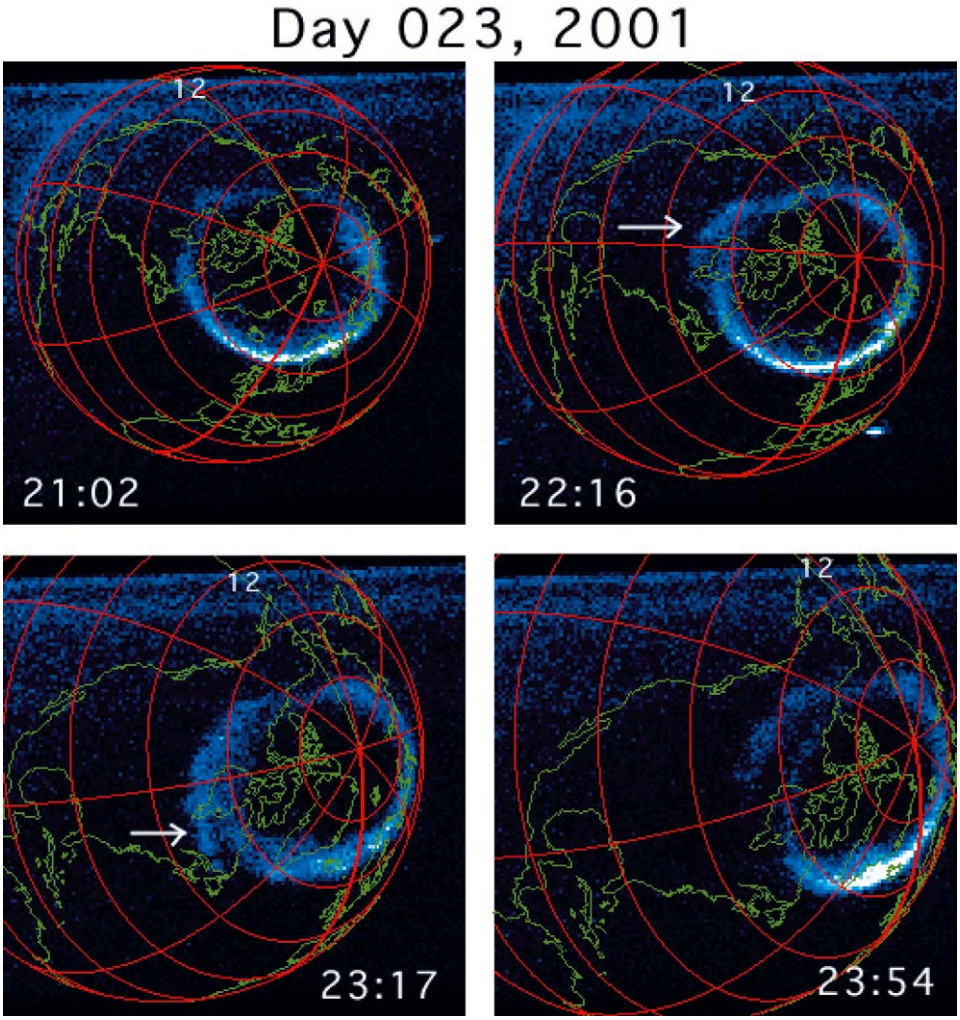

Figure 7. SI-12 images between 21:02 UT and 23:54 on January 23, 2001. The direction to the sun is indicated by the meridian labeled 12. Significant separation of an equatorward arc from the main oval is indicated with arrows at 2216 and 2317 UT.

1979]. These aurorae took the form of bands and diffuse arcs extending over several hours of local time in the dusk-evening sector. These studies characterized the precipitation as electron aurorae, from comparisons of the emissions of OI and N_2^+, and from some in situ measurements of precipitating particles. The proton fluxes were found to be relatively inconsequential. New studies of this phenomenon are now possible using the spectrographic imaging component of the Far Ultraviolet Imager on the IMAGE satellite [Mende *et al.*, 2000; Burch, 2000].

An example of SI-12 images of this phenomena were obtained starting at 1325 UT on January 23 (day 23), 2001 until the end of the day, during which IMAGE

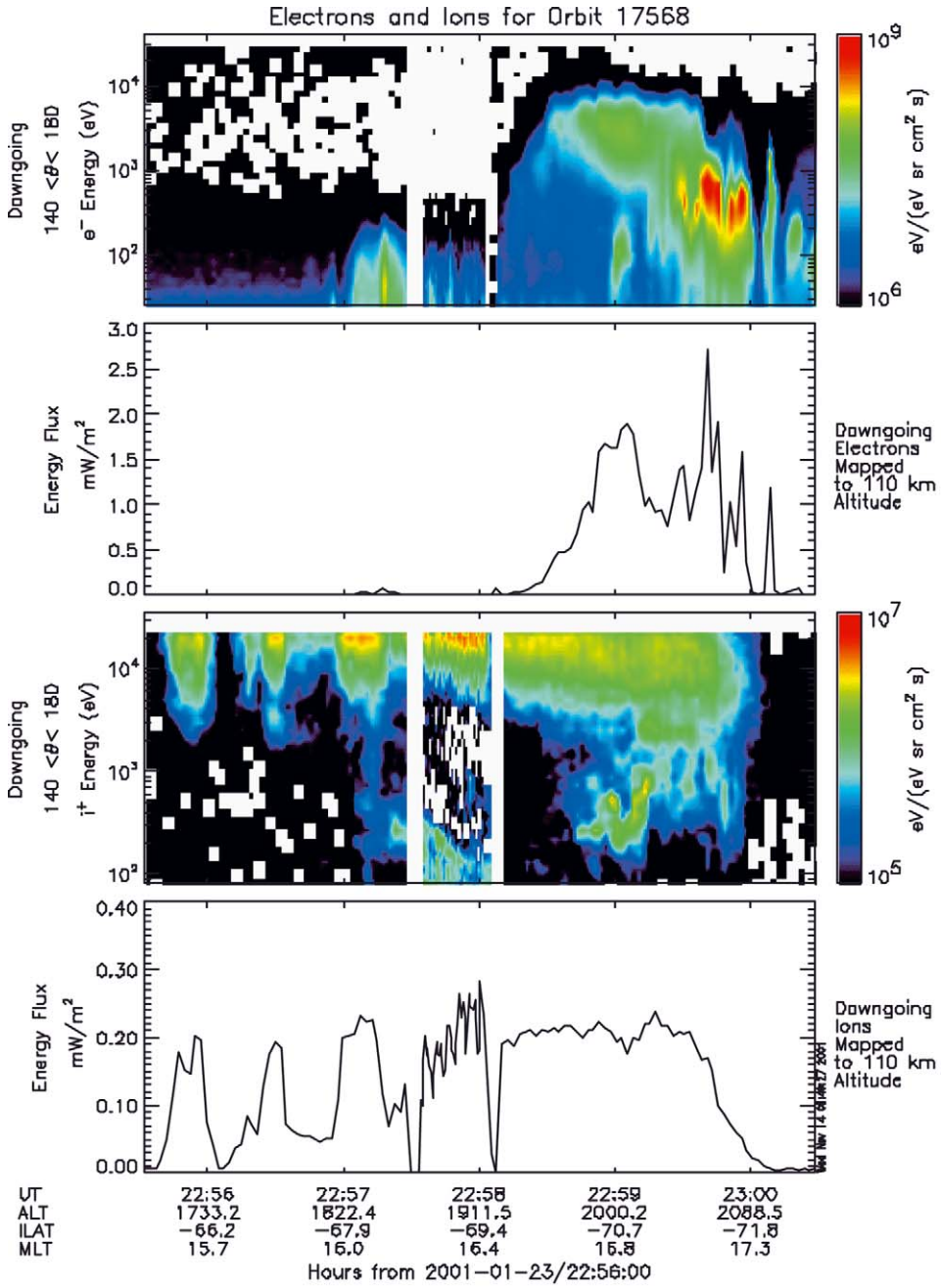

Figure 8. Energy spectrograms of precipitating electrons and protons as measured by the FAST electrostatic analyzer, conjugate to the IMAGE observations shown in Figure 7. The differential flux of electrons with pitch angles between 140° and 180° (precipitating), and the corresponding total energy flux are shown in the first and second panel, respectively. The same parameters from the ion measurements are shown in Panels 3 and 4.

had a continuous view of the entire oval. Selected images of the proton aurora are shown in original image coordinates in Figure 7. The meridian annotated with the number 12 shows midday. The signature of subauroral precipitation became apparent in the afternoon sector beginning around 2100 UT, separate from higher latitude auroral precipitation, but basically still connected to the main oval at noon. The feature is very distinct at 2216 UT. Around 2300 UT, the dusk sector proton aurora brightened considerably, followed by a dramatic separation of the auroral arc, where the equatorward portion separated completely from the oval and propagated to 65° magnetic latitude, while the main oval receded several degrees towards the pole.

Observations of several of these bright signatures of proton precipitation show that they are often centered over the afternoon sector of local time, where the strongest emissions are observed in the 1500-1700 MLT range. From these global images, one can also discern an apparent correspondence between the nightside proton auroral brightness and the appearance of dayside subauroral forms. At times 35–50 min prior to the most pronounced subauroral proton signatures, there are clear signatures of the enhancement in the dusk-midnight proton auroral oval brightness and its latitudinal extent [Immel *et al.*, 2002].

FAST is a polar orbiting satellite dedicated to making high-time resolution measurements of particle precipitation and electric and magnetic fields in the auroral environment [Carlson *et al.*, 2001]. On day 23, 2001 at times between 2255 and 2300 UT, the satellite was in the 15-17 MLT sector, at magnetic latitudes between -65 and $-72°$. These are locations exactly conjugate to the subauroral enhancement observed in the northern hemisphere by IMAGE-FUV. Measurements of the electron and proton energy spectra from the FAST electrostatic analyzers are shown in Figure 8 as a function of UT, MLT, and magnetic latitude. The top panel shows the differential energy flux of precipitating electrons with pitch angles between 140 and 180° (i.e. downward because the magnetic field in the southern hemisphere is pointing upward. The second panel (Figure 8) shows the integrated electron energy flux over these precipitating loss cone angles from the differential measurements. Like plots for the ion precipitation are shown in Figure 8 third and fourth panels.

The FAST data show a remarkably structured signature of significant proton precipitation, with three peaks in the energy flux at -65.5, -67.0, and $-68.2°$ magnetic latitude. Assuming a Maxwellian distribution of energies, the mean energy per proton is found to be between 24 and 32 keV at these three locations. A fit with a kappa function used in the IMAGE- FUV calibration and modeling results in a 10–20% increase in these mean energies, depending on the value of kappa. However, without measurements at energies > 30 keV, such fits are not possible. Because of this limitation, the integrated precipitating energy flux observed by FAST is approximately a third to a fifth of the total precipitating energy flux. Therefore, the peak proton energy flux that one would infer from the FAST observations of 0.2 mW/m^2 is $\sim$1.0 mW/m^2.

It is clear from the FAST measurements of the electron energy spectrum and flux (Figure 8 top two panels) that no electron precipitation caused emission, bright enough to be detected by WIC, is observed equatorward of 69.5° magnetic latitude. Therefore, the WIC and SI-12 imagers provide two independent measurements of the emissions produced by the sub-auroral proton precipitation. Using the work of Hubert *et al.* (2001), the LBH emissions created by a proton aurora can be compared with its Lyman α emissions to estimate the mean energy and total energy flux of the protons.

At the time of maximum equatorward extent of the subauroral precipitation concurrent WIC and SI-12 images were mapped to geomagnetic latitude and local time coordinates. Line plots of the counting rates in each channel at the 1600 MLT meridian between 50 and 90 degrees magnetic latitude were compared. The signature of the subauroral precipitation in the afternoon sector was clear in both SI-12 and WIC line plots extending from 1300 to 1800 MLT, with a peak in brightness near 1600 MLT at 64° magnetic latitude. WIC counting rates were also calculated by modeling the estimated contribution of the proton produced emission including the secondary electrons produced emissions (after Hubert *et al.*, 2001). Two cases were considered assuming proton mean energies of either 8 keV or 20 keV. From this it was shown that proton precipitation of 20 keV would produce enough LBH emissions to account for the response of the WIC camera over most of the subauroral form. Indeed, the proton aurora must account for all of the emissions equatorward of ∼70°, as there is no significant electron precipitation at these latitudes. The proton energy flux inferred from the optical data along this meridian is 1.2 mW/m^2 peaking at 64°.

It should be noted that for the purposes of this type of calculations the dayglow emissions had to be removed by using an empirically derived dayglow response model for each instrument [Immel *et al.*, 2000]. The dayglow correction is small when compared to the counting rates from auroral emissions, particularly in the SI-12 channel, but is necessary to achieve the best determination of precipitating energy.

Using IMAGE SI-12 data Zhang *et al.* (2003) discuss several observations of Dayside Detached Auroras (DDA-s). Simultaneous DMSP overpasses permitted the analysis of the particles causing these subauroral features and in most cases it was found that they were protons.

4. Discussion of subauroral proton precipitation

The appearance of subauroral proton precipitation in a dayside local time sector shows little similarity to any previously studied subauroral proton event. The morphology of these auroral features compares well with the local time and latitude of auroral signatures observed by ISIS-2 [Moshupi *et al.*, 1979]. However, contrary to the ISIS-2 observations, we find that protons are the primary component of the

precipitating particle population. The N_2 LBH emissions that are usually associated with electron aurora are due, in this case, entirely to precipitating protons. These events are relatively rare, but often associated with a high dynamic pressure in the solar wind. In several instances a clear signature was seen to extend over more than 1 hour of local time. The mean energies observed by IMAGE and FAST are consistent with protons, which drift around the dusk sector after injection from the magnetotail near midnight [DeForest and McIlwain, 1971]. These populations can either continue to drift as a part of the ring current, precipitate into the atmosphere, or exit the magnetosphere at some dayside local time sector. This behavior depends on the electric fields within the magnetosphere, the degree to which the solar wind has compressed the magnetopause, and the effectiveness of the initial injection in driving these protons to low L-shells. The morphology of the subauroral forms observed by IMAGE-FUV varies, but they often are connected to the auroral oval near noon, reaching lower latitudes further into the afternoon sector. Traced out along magnetic field lines to the magnetic equator, this corresponds approximately to drift paths of 24-32 keV protons, which travel close to the Earth in the dusk sector and closer to the magnetopause at noon.

Clearly it is relatively easy to account for the presence of the particle source at these latitudes however the main question is what special circumstances occur which cause the particles to precipitate. The mechanism by which these protons are caused to precipitate must be explained, and there are several possibilities. An enhancement of the abundance of cold plasma in the ring current can cause the growth of the electromagnetic ion cyclotron (EMIC) instability, forcing ring current ions into the loss cone [Brice and Lucas, 1975, and references therein]. With the enhanced capabilities of the IMAGE satellite one might expect to observe this as an enhancement in the plasmaspheric density in the IMAGE EUV images, which show the HeII component of the plasmasphere [Sandel *et al.*, 2001]. This could show in the form of a plasmaspheric bulge or a dense, sunward-directed tail. In the case presented here such a tail was not observed, but the cold plasma densities required for instability growth (10-10^2 HeII/cc) are near the sensitivity threshold of the EUV instrument. Recent modeling of large magnetospheric storms shows that EMIC waves can contribute significantly to ion precipitation in the afternoon local time sector [Jordanova *et al.*, 2001]. Another possible mechanism for loss-cone filling is the presence of a parallel electric field, but no evidence for this is seen in the FAST proton spectra.

Another scenario could be an increase in the proton density and or a redistribution of the trapped protons due to external causes such as a compression of the magnetopause, and the wave generation and ion heating [Anderson and Hamilton, 1993]. In some cases subauroral proton precipitation has been observed by the SI-12 imager in conjunction with the arrival of shocked solar wind at Earth [Zhang *et al.*, 2003]. However the solar wind density and velocity was only varying slowly during the time of this study and compression does not appear to be a factor. Possibly more significant is the steady northward turning of the IMF between 1800

and 2200 UT, which causes the auroral oval to retreat to higher latitudes, and may also provide the trigger for the nightside proton injections. The favorable timing of these two phenomena may work to exaggerate the difference between the high-latitude and subauroral emissions, as has been shown in other cases by Burch *et al.* [2002]. How the protons are caused to precipitate in regions separate from the auroral oval with the periodic arc-like structure observed by FAST, and how these observations relate to the detached electron aurorae observed with ISIS-2 are still open questions.

Zhang *et al.* (2003) were able to correlate the occurrence of DDA with sudden solar wind dynamic pressure enhancements and northward IMF. DDA-s are usually very dynamic and short-lived with a lifetime on the order of 10 minutes. DDA are best detected by the IMAGE FUV SI-12 indicating that energetic proton precipitation is the major component. Simultaneous DMSP particle observations confirm energetic protons (>10 keV) in the dayside inner magnetosphere. In some cases DMSP also detected significant electron fluxes associated with DDA. Precipitations of energetic protons (electrons) which caused DDA could be explained by enhanced cyclotron instability which arose from adiabatic compression following sudden solar wind dynamic pressure enhancements.

Zhang *et al.* (2003) found that northward IMF is a necessary condition for DDA occurrence. Occurrence of DDA can be well explained by a model proposed by Zhou and Tsurutani (1999) that solar wind dynamic pressure enhancements caused increase of proton/electron's temperature anisotropy leading to cyclotron instability which diffused protons/electrons into a loss cone [Zhang *et al.*, 2003]. Short lifetime of DDA may be due to slow replacement of precipitated protons/electrons from the nightside magnetosphere under northward IMF condition. Both protons and electrons, which are found occasionally in these events, have the same energy range, indicating no field-aligned acceleration. This further confirms that the precipitated protons/electrons were due to wave scattering.

These observations by IMAGE-FUV show a newly discovered phenomenon, which only now can be observed in a global sense. The SI-12 imager observed enhanced proton precipitation separate from the auroral oval over several hours of local time in the afternoon sector. It is clear from the FAST data that the subauroral arcs are purely the result of precipitating protons, which can be represented by a Maxwellian energy distribution with a 24-32 keV mean energy.

In summary, detached proton arcs appear after a favorable combination of events. These include a strong injection of protons from the magnetotail and large positive changes in IMF B_z.

5. Nightside auroral observations: Proton auroras and substorms

Detailed understanding of precipitating proton morphology would answer many of the key questions regarding substorms. Precipitating protons in the energy range

>10 keV are only marginally affected by the electric fields which are thought to drive most electron auroras. Precipitating protons signify the presence of trapped protons on the field line coupled with some mechanism which fills the loss cone by efficiently isotropising the protons. Thus the presence of precipitating protons prior to substorm onset would signify the presence of hot plasma in the inner magnetosphere.

The key to understanding substorms is the description of the instantaneous magnetospheric configurations during its phases. To relate the extensive information available from low-altitude satellite and ground-based observations to those made in the magnetotail plasma sheet requires knowledge of the dynamic magnetospheric configuration. It is difficult to identify the magnetospheric source regions of auroral arcs and different types of particle precipitation from simple field line mapping [Siscoe, 1991]. Mapping the equatorial plasma sheet to conjugate ionospheric regions is limited because the two regions are decoupled in several ways. Quasi-static electric fields and other complex accelerating forces modulate the particles at low altitudes. During substorms when large re-configurations take place additional complications arise because the electric fields do not map in the presence of the inductive electric fields. These forces change the character of low energy electrons and protons between the plasma sheet and the ionosphere. Direct empirical field line models [Tsyganenko, 1990] are more useful characterizing the average field but they are limited in their value in predicting instantaneous configurations. For example they seriously under estimate the degree of field line stretching during substorms. Sergeev and Malkov (1988) proposed an indirect method of probing magnetic field gradients via remote sensing by low altitude spacecraft. They determine from low altitude satellite the position of the isotropic boundary (IB), the region where the particles become isotropic i.e. fill their loss cone. This is then interpreted as the boundary between the adiabatic and stochastic particle motion in the equatorial tail current sheet [Sergeev *et al.*, 1993]. By measuring the particle pitch angles on low altitude satellites it is possible to adjust the magnetic field model so that the low latitude boundary of the region of stretched field lines coincides with the IB. By comparing low altitude satellite particle data with GOES-2 synchronous altitude magnetic field data Sergeev *et al*. [1993] show that the low latitude IB position for 30 to 300 keV protons is strongly controlled by the equatorial magnetic field in the tail.

IMAGE SI-12 measurements will allow global interpretation of the IB as the equatorial edge of the dominant energy precipitating protons boundary. The behavior of proton precipitation during substorms has a potential of resolving some of the key questions regarding substorm processes. The magnetospheric counterpart of the poleward boundary of the proton precipitation in the magnetosphere is less well understood. It is most likely to be the poleward boundary of the intense part of the trapped proton fluxes. Proceeding further outward one enters the region of pre-substorm poleward electron precipitation. The connectivity of this region is still somewhat uncertain at this point. Proceeding further after the most poleward

electron arc we arrive at the zone of the polar rain which clearly signifies that the field lines are permanently open. At substorm onset the system reconfigures and our global 'proton and electron images' will be helpful in interpreting the substorm process.

Montbriand [1971] and Eather *et al.* [1976] found that diffuse electron precipitation is collocated with the proton aurora. During the substorm growth phase, the proton aurora moves equatorward accompanying the development of the ring current and it is absent in the leading edge of the expanding substorm auroral bulge in the pre-midnight region [Fukunishi, 1975]. In the substorm growth phase the diffuse proton aurora lies equatorward of the discrete aurora in the pre-midnight region [Vallance Jones *et al.*, 1982] and at substorm onset the poleward boundary of the proton aurora can reach near that of the electron aurora. From monochromatic all sky camera observations Mende and Eather (1976) found that the bright part of the westward surge does not contain proton precipitation and the proton aurora expands poleward to occupy a large diffuse region poleward of the pre-substorm position. Samson *et al.* (1992) observed that the electron arc that brightens at substorm onset is located within a region of intense proton precipitation with energy that monotonically increases with decreasing latitude. The auroral arc that intensifies at substorm onset often forms on magnetic field lines that map to within the geosynchronous region [Lyons and Samson, 1992]. Deehr (1994) showed that in 33 substorms the electron arc is always poleward of the proton arc at onset and that this conclusion is less pronounced toward midnight (MLT). Proton precipitation is evidence for closed magnetic field region [Samson *et al.*, 1992] and the development of protons might shed light on the location of the boundary of the closed field line region during substorms.

Takahashi and Fukunishi (2001) found from ground-based observations that although the protons do not populate the substorm surge they tend to expand poleward with the surge. They also find that there are large Doppler shifts in the proton aurora at the poleward surge boundary suggesting that the protons are highly energetic.

In Figure 9 we show one of the first substorms which was observed by the IMAGE satellite by showing a sequence of WIC (left) and SI-12 (right) images [Mende *et al.*, 2001]. The noon-midnight meridian is very closely aligned with the vertical of the page (midnight is approximately at the top). The grid is geographic with 75, 60 and 45° latitude circles and is used to facilitate the intercomparison of the auroral locations in the WIC and SI-12 images. The WIC images were scaled with a single set of scaling parameters to optimize the brightness and contrast of the presentation and to preserve the relative brightness of the images in the sequence. The WIC images are displayed on a red-to-yellow-to-white color palette. The SI-12 images were scaled to a blue-light blue-green color palette. No dayglow or other corrections were applied to either image. In the WIC images the dayglow is significant and the auroras are superimposed on it and can appear brighter on the day (sunlit) side than on the night side.

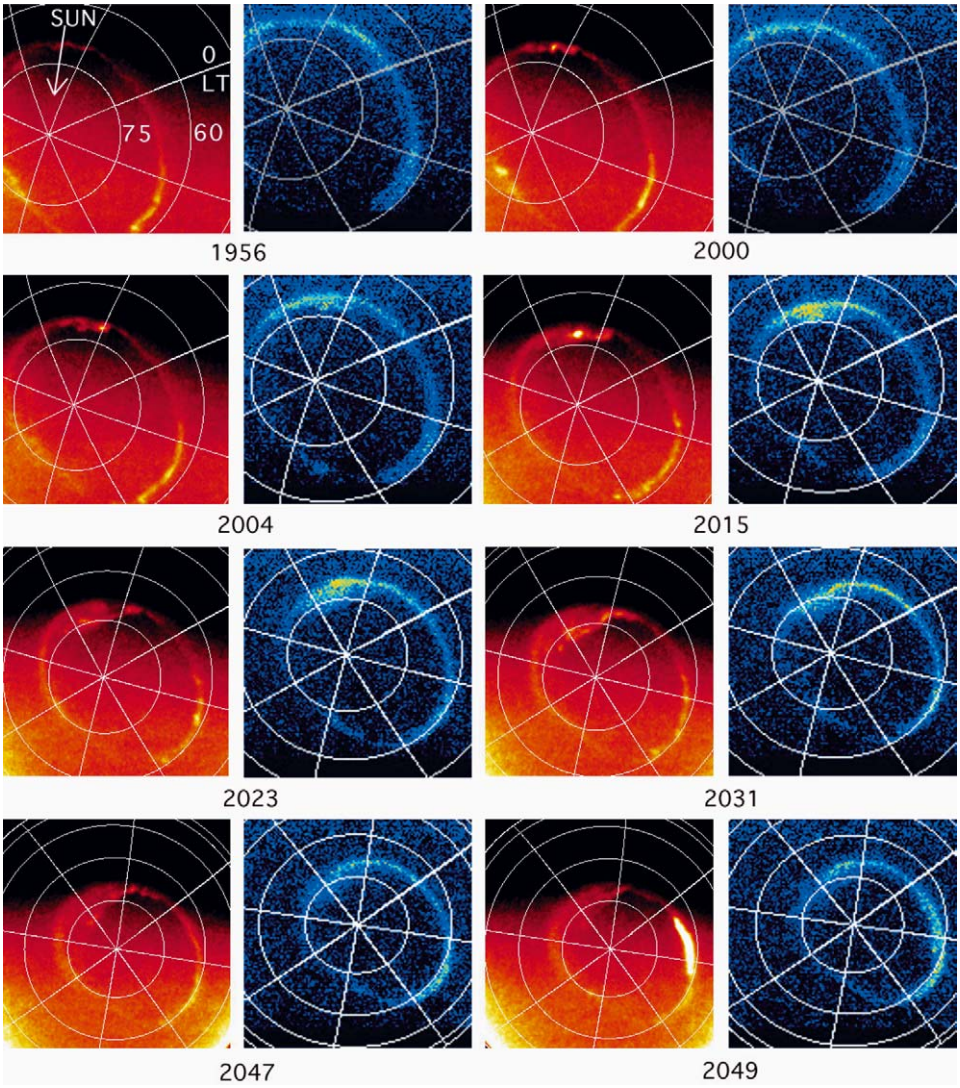

Figure 9. Geographic projection of the IMAGE Wideband Imaging Camera (WIC left shown in red) and the Spectrographic Imager SI-12 channel (right shown in blue) from 1956 to 2049 UT on Day 180, 2000 [Mende *et al.*, 2001]. The WIC images represent overall precipitation (mainly electrons) and the SI-12 channel represents Doppler shifted hydrogen i.e. proton precipitation. The sun direction and the geographic latitude local time meridians were annotated on WIC frame 1956.

At 1956 the aurora was quiet with very little activity in broad band LBH (WIC) except the early afternoon where we see evidence of some structuring in the form of possible Kelvin Helmholtz waves or perhaps large spacing spatially periodic auroral distortions [Vo and Murphree, 1995]. The proton aurora was fairly uniform, diffuse with a peak intensity of ∼35 counts (corresponding to about 1 to

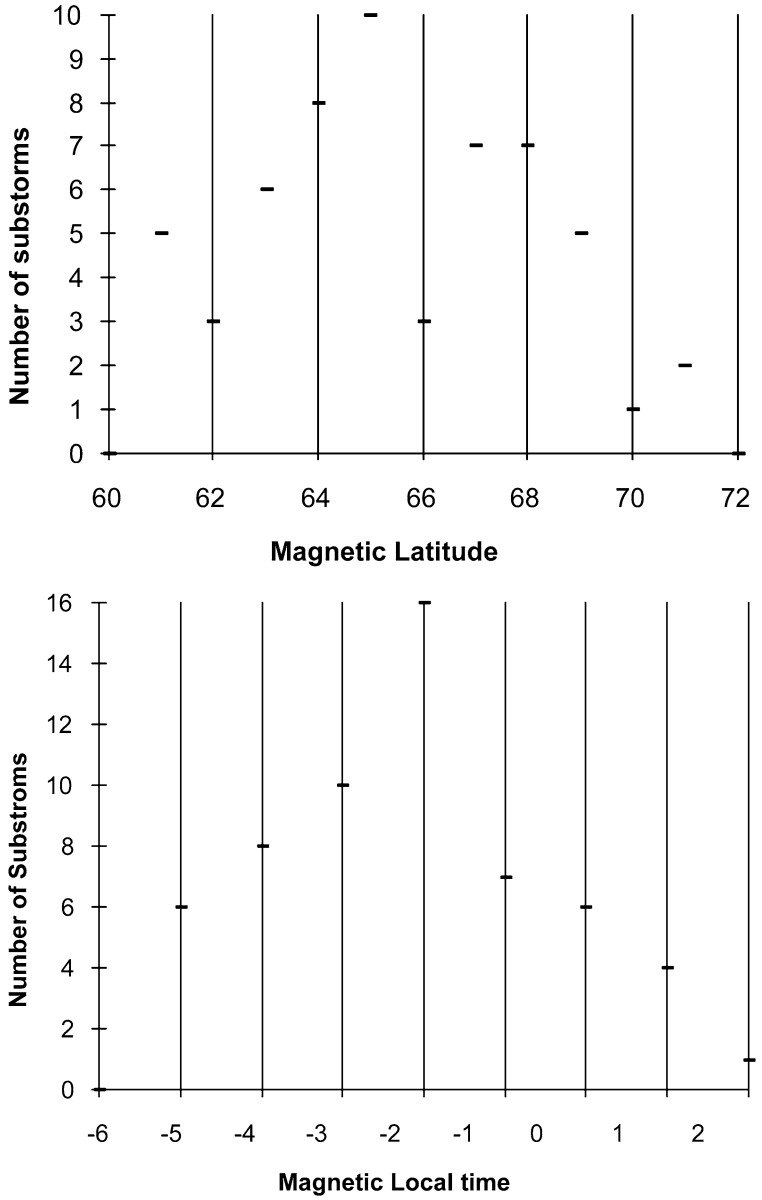

Figure 10. Number of substorms (a) in one degree magnetic latitude bins and (b) in one hour magnetic local time bins.

1.5 mW/m^2 mean precipitated energy of 8-25 keV protons). It is located slightly equatorward of the electrons on the dusk/evening side but seems to be collocated with the electrons at midnight. The first sign of a breakup is seen as a spot in the WIC image near midnight at 2000 UT.

The first response of the proton aurora to the substorm is a poleward expansion near midnight (2004) when the WIC signature is relatively weak. The 2004 bright spot in the WIC does not have a counterpart in the SI-12 image. The poleward boundary of the protons perhaps leads the poleward boundary of the electron surge (2015) and the SI-12 aurora almost touches the 75° latitude circle while the electron aurora is still at 72° or 73°. At 2023 UT there is a faint region of proton precipitation, which is at as high or higher latitude than the brighter electron surge, however the bulk of the proton intensification takes place at the original location of the proton aurora. The proton count rate by this time increased from 36 counts to 45 counts per exposure per pixel ($\sim$ 2 mW/m^2).

At 2031 the poleward surging WIC aurora is brightest at the poleward edge of the surge while the SI aurora is brightest equatorward and duskward. At 2047 the electron aurora reaches its highest latitude and the SI-12 aurora is distinctly left behind. It is also clear that at this time the proton aurora is absent in the leading edge of the expanding electron auroral bulge [Fukunishi, 1975; Mende and Eather, 1976]. On the night side the protons fill the evening dusk of the oval and the electrons mainly fill the dawn side in agreement with the azimuthal drift of midnight injected electrons and protons. A sudden brightening occurs in the dusk sector at 2049 but this does not appear to be spatially related to this substorm.

Based on the IMAGE FUV data from a single case substorm study Mende *et al.* [2001] concluded that in the pre-substorm phase at early evening local time the proton aurora was equatorward of the electron precipitation and near midnight they were collocated. The sudden brightening of the aurora at substorm onset near midnight was seen mostly in the electrons although there were protons present at this location. During the expansive phase both the electrons and protons expanded poleward. The electron aurora formed a bright surge at the poleward boundary while the protons showed diffuse spreading. The peak intensity of the protons did not change substantially during the entire event. In this substorm the proton aurora is brighter on the dusk side while the electron aurora is on the dawn side. Later as the electron surge expanded poleward it left the protons behind. The electrons formed a discrete auroral feature near the aurora-polar cap boundary, which was devoid of substantial energetic ($>$1 keV) proton precipitation. The presence of precipitating protons at the point where the initial brightening is seen shows that the substorm was initiated on closed field lines.

The large body of IMAGE FUV data permits putting the above conclusions on a firmer statistical basis. To facilitate this study we have performed a superimposed epoch analysis of substorms. Superimposed epoch analysis of substorms have been performed in several studies: Caan *et al.* (1975); Rostocker *et al.* (1984); Samson and Yeung (1986) and most recently by Newell *et al.*, (2001) based on the POLAR

UVI data. Newell *et al.* studied 390 substorms and calculated the auroral power dissipation during the substorm events. They have examined the auroral power dissipation as a function of magnetic local time and found that the most intense power increase in the pre-midnight sector is a factor of 3.4 during the first 9 minutes. They found that the most dramatic energy change is in the vicinity of the onset and it becomes less dramatic as the aurora is further away. They found minimal effect on the dayside except a slight reduction of auroral intensity perhaps due to the decrease in magnetospheric electron population [Gorney and Evans, 1987]. They also found a 10% reduction in auroral power prior to substorm onset. Because of the narrowness of the POLAR UVI field of view they had to use images, which were not truly global. Although our database from IMAGE observations is smaller, 59 substorms, we only used images where the entire auroral oval was visible. Our analysis of the IMAGE FUV observations also permitted the comparison of the protons with the electrons.

Substorms with good IMAGE coverage were selected. IMAGE satellite apogee was essentially above the North Pole during these observations permitting a long period of uninterrupted observations in each orbit. The intensity of the images during the selected substorms was plotted in a rectangular magnetic latitude (ML) and magnetic local time (MLT) frame. In these ML-MLT plots the x coordinate axis was magnetic local time, the y axis was magnetic latitude and the z axis or brightness represented the instrument count rates. We have used bin sizes of 1 degree ML and 15 minutes MLT. Such an ML-MLT plot was generated from each of the WIC and SI-12 images representing the global auroral situation every 2 minutes. The relatively large signal to noise ratio of the WIC imager permitted reliable determination of the sudden initial brightening which continued to spread in MLT and persisted for at least 30 minutes. The onset locations (ML and MLT) and times (UT) were thus determined by manual inspection of the WIC images. The number of onset points in our substorm set are presented as a function of magnetic latitude in Figure 10a. Similar plot for magnetic local time is shown on Figure 10b. For each substorm ML-MLT plots were made every two minutes starting 30 min before onset and ending one hour after.

For the superimposed epoch analysis the above described ML-MLT plots were shifted along the x (MLT) axis until the starting point of each substorm ended up at the middle of the 24 hour frame i.e. at 0 relative local time. In the resulting plots the x coordinate represents the relative magnetic local time (RMLT) that is relative to the local time of substorm onset.

It was necessary to find suitable parameters to describe the properties of the aurora for our statistical analysis. In addition the WIC images were superimposed on a varying intensity of dayglow background. To eliminate the dayglow and to find significant parameters to describe the latitude position and extent of the aurora we fitted a Gaussian along the vertical (magnetic latitude axis) at each local time region in each ML-MLT frame. The spatial resolution of our global images was limited to about one degree of latitude and a single Gaussian function of latitude provided

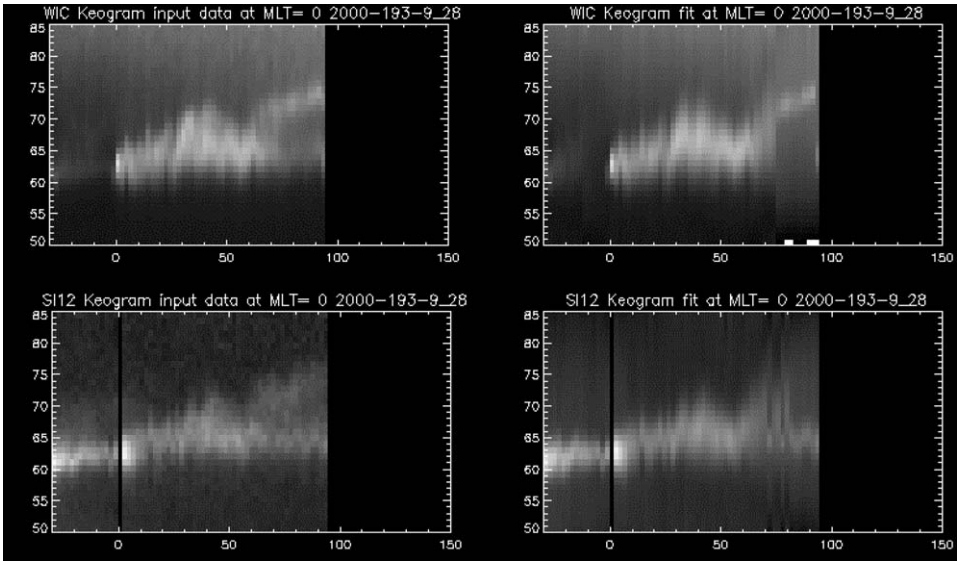

Figure 11. A typical substorm example (year 2000, day 193 hour 09:28 UT) displayed in the conventional Keogram format at the magnetic latitude of the onset. The top Keograms are WIC and the bottom ones are for the SI-12. On all Keograms the x and y axes are UT time in minutes with T=0 at substorm onset and magnetic latitude in degrees respectively. Left Keograms are magnetic latitude/MLT projected input data in instrument output units (AD units for WIC and photoelectron counts for the SI-12). On the right the data is shown as a fitted Gaussian along each magnetic meridian.

an equivalent auroral latitude intensity profile that was a good representation of the data in most cases. The Gaussian had the form of:

$$z = a_0 \exp(-(y - a_1)^2/a_2)/2 + a_3 + a_4 y + a_5 y^2$$

where y is the magnetic latitude and z is the intensity. The coefficients a_0, a_1, a_2, represent the auroral intensity peak, latitudinal position of the peak, latitudinal width respectively while a_3, a_4, and a_5 represent the airglow background as it varies with latitude. For each fit we used a goodness of fit criteria, which required that the sum of the square of the deviations, the differences between the fitted and the actual data, was less than the sum of the square of the data multiplied by a coefficient. The coefficient was 0.001 for WIC and 0.1 for SI12. Excluding situations when there was missing data due to bad view angles, in almost all situations, the fit converged and the criteria was met.

By selecting a particular relative magnetic local time, for example RMLT = 0 (MLT of substorm onset) we can plot the vertical (magnetic latitude) profile of the intensity as a time series. This was done on Figure 11 for the input data for WIC (top left) for the Gaussian fit of the same data (top right) and for the SI-12 data bottom left and the Gaussian fit bottom right for a substorm which occurred on day 193, 2000 at 09:58 UT.

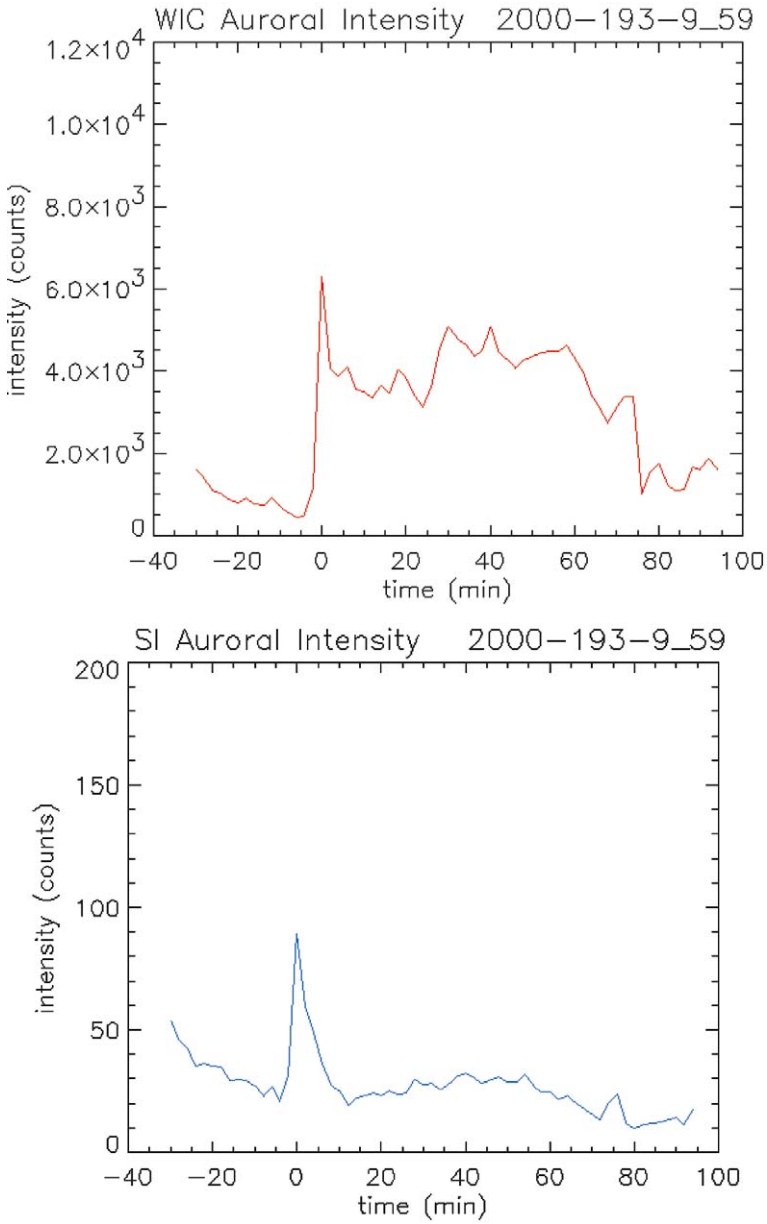

Figure 12. Typical example of substorm plots. (a) WIC intensity (a_0) from 30 minutes before onset to 90 minutes after. (b) is SI-12 intensity. (c) is the latitude center parameter (a_1) for WIC crosses and SI asterisks respectively. (d) is the Gaussian width parameter (a_2) for WIC, crosses and SI-12, asterisks. On all plots, the x axis is UT time in minutes with T=0 at substorm onset and the y is either corrected instrument count rate or magnetic latitude in degrees

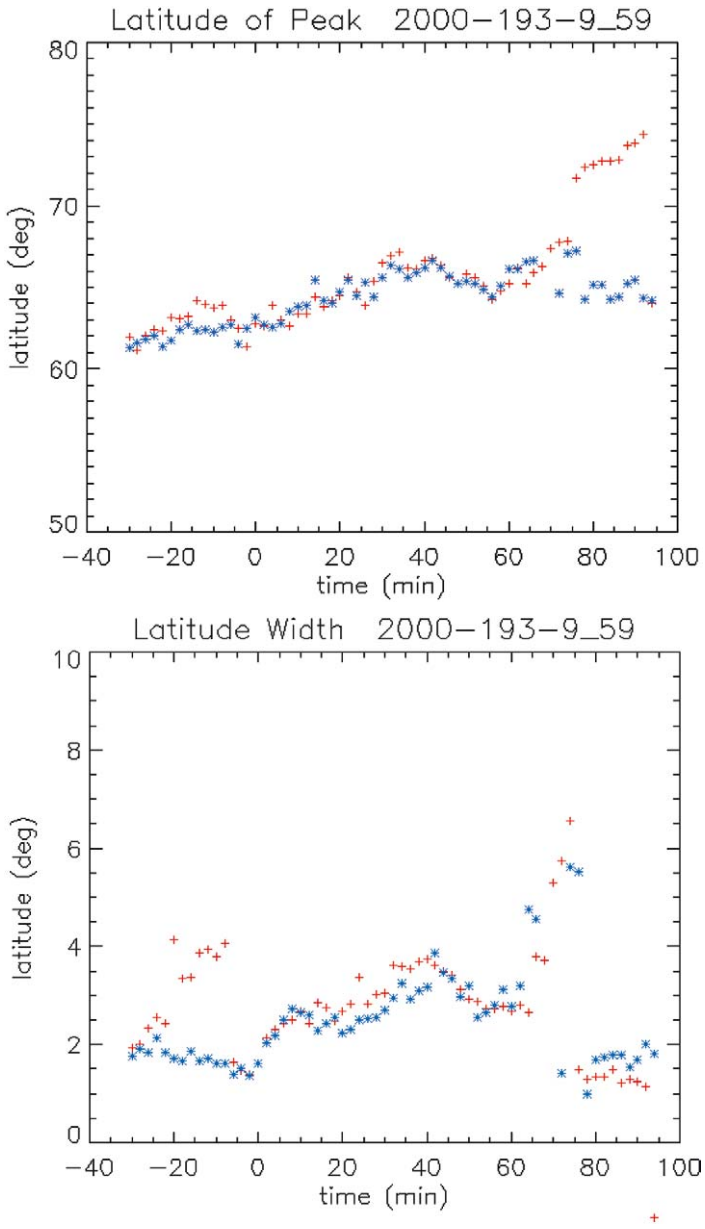

Figure 12. Continued.

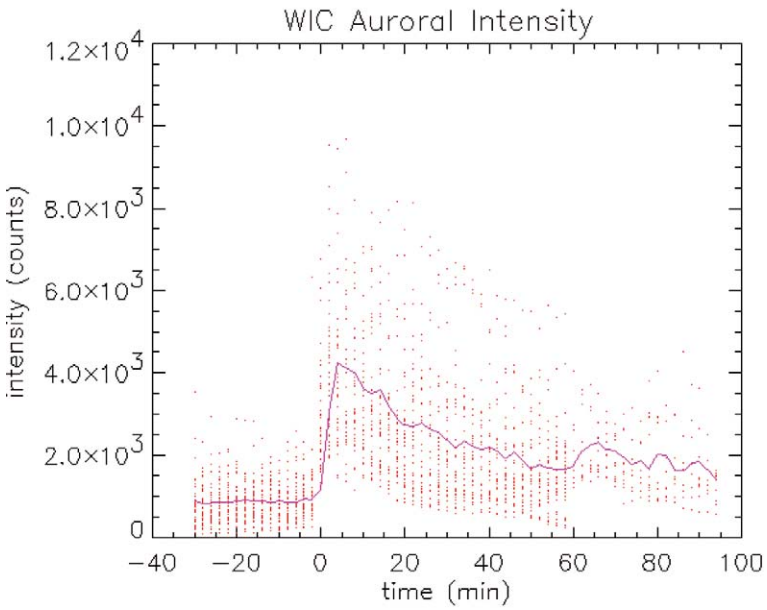

Figure 13. Scatter plot for the selected substorm set. WIC intensity (a_0), WIC corrected counts, from 30 minutes before onset to 90 minutes after. Solid line is the mean.

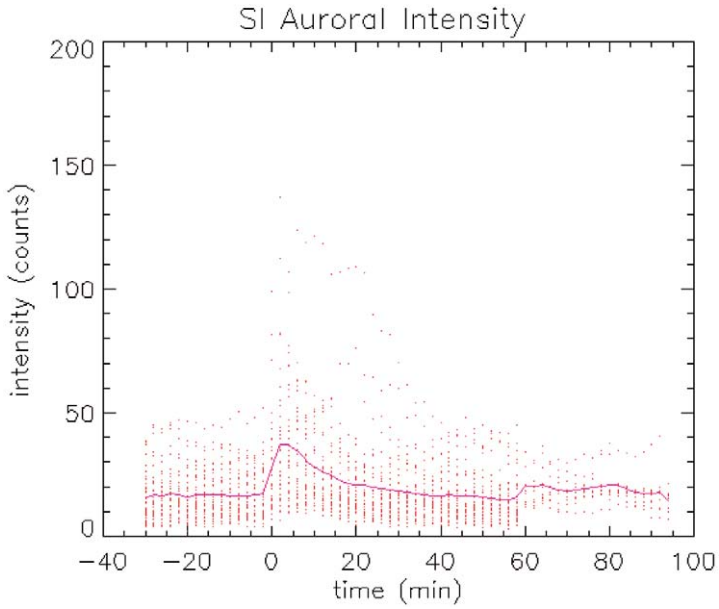

Figure 14. Scatter plot for the selected substorm set. SI-12 intensity (a_0) SI-12 corrected counts from 30 minutes before onset to 90 minutes after. Solid line is the mean.

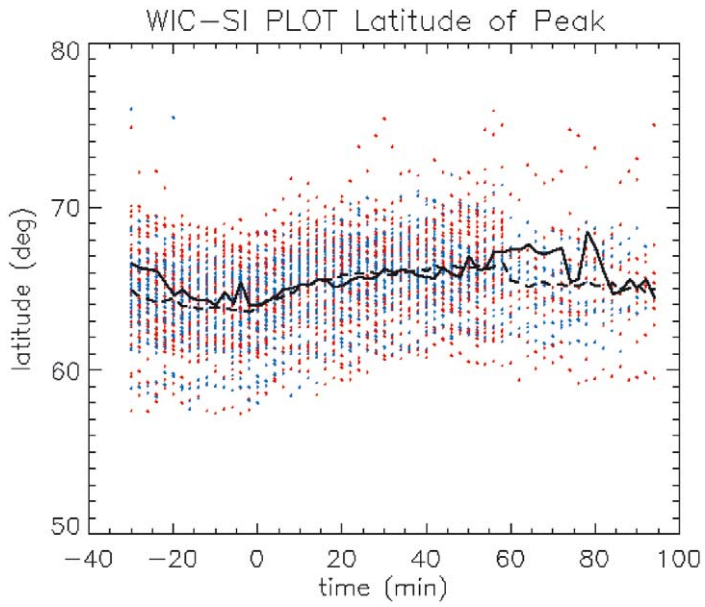

Figure 15. Scatter plot of the latitude center parameter (a_1) in degrees ML for WIC (red) and SI-12 (blue) from 30 minutes before onset to 90 minutes after. The mean is indicated with a solid and a broken line for WIC and SI-12 respectively.

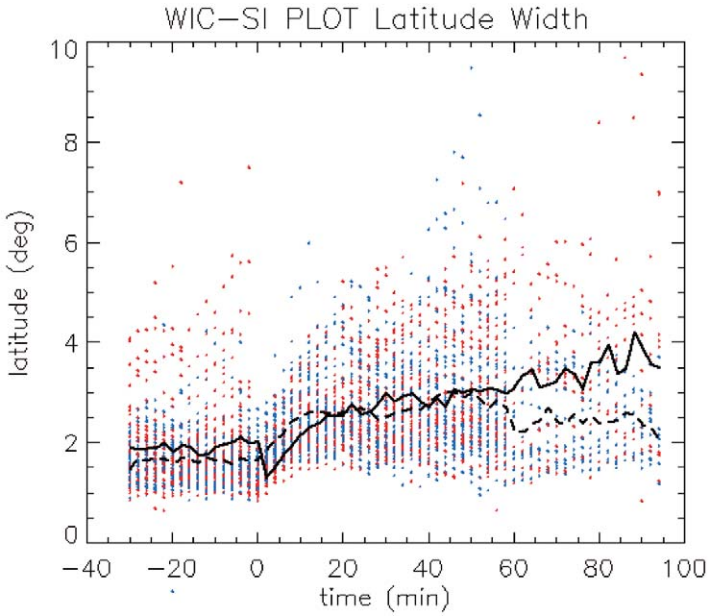

Figure 16. Scatter plot of the Gaussian width parameter (a_2) for WIC (red) and SI-12 (blue) from 30 minutes before onset to 90 minutes after.. The mean is indicated with a solid and a broken line for WIC and SI-12 respectively.

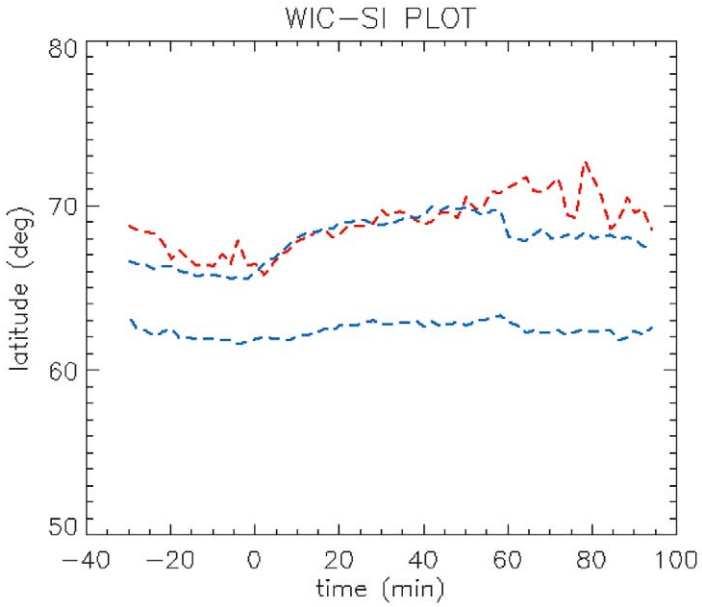

Figure 17. The mean latitude (in degrees) of the equatorward boundary of the equivalent SI-12 counts (IB), the mean latitude of the poleward boundary of the SI-12 counts and the poleward boundary of the WIC counts (Polar Cap Boundary) from 30 minutes before onset to 90 minutes after.

This format is identical to the auroral latitude, time, intensity plot format introduced some years ago as a Keogram [Eather *et al.*, 1976]. In general the Gaussian fits on the right are extremely good representation of the original data on the left. However it should be pointed out that the Gaussian fit is not a perfect representation of the data. For example on the right side of the Keogram at T > 60 min the aurora separates into a double oval configuration whereas the Gaussian fit treats it as a single peak. Although it is important to take notice of such limitations, this technique provided a simple characterization of the aurora while effectively removing the dayglow contributions. We will proceed by describing this one substorm in terms of the Gaussian description and then we will discuss the average properties of the entire substorm set.

In Figure 12 we present typical plots for the same substorm denoted by the onset time of year 2000 day 193, 09:59 UT. The plots start 30 min prior to substorm onset or 09:28. All plots were made at RMLT of zero that is on the meridian of the substorm onset. Figure 12a is the WIC intensity plot, or more precisely the plot of the a_0 Gaussian coefficient. The substorm intensification at T = 0 is from WIC counts of about 1000 to about 6000 at the peak after the onset. It should be noted that the quantity plotted here represents the Gaussian peak intensity at RMLT = 0 regardless of the latitude position or width of the aurora. Figure 12b is the same plot but for the SI-12 proton precipitation. A sudden increase of a factor of ∼4 is noted. Figure 12c represents the latitude position of the Gaussian

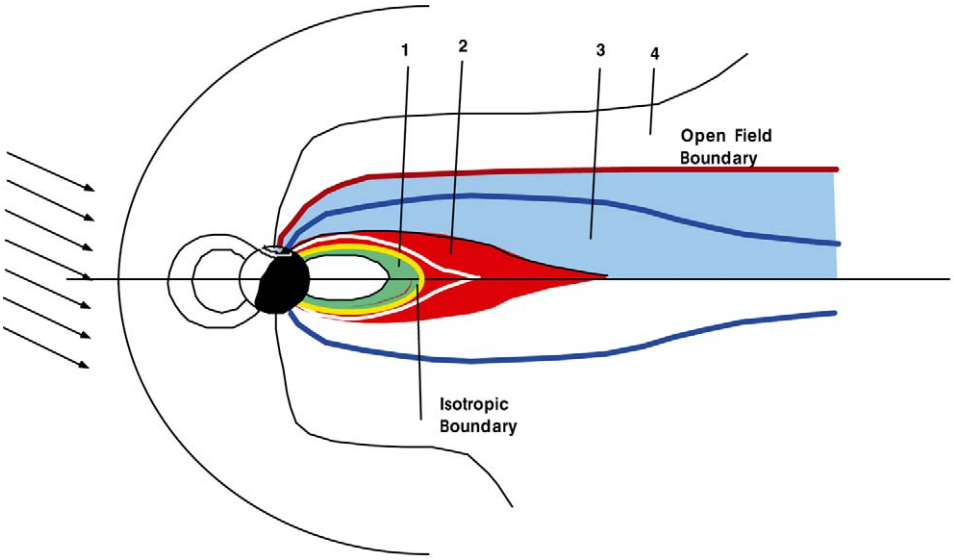

Figure 18. Schematic representation of the various nightside magnetospheric regions. The inner region (green, region 1) contains non precipitating trapped ring current protons. The red region (region 2) represents intense proton precipitation where the field lines are distorted and the protons are randomized by the equatorial field configuration of the stretched field lines. The boundary between the red and green region is the isotropic boundary or IB. Outside the red region the proton precipitation is below the threshold of the imager ~0.1 mW/m^2. This blue region (3) probably expands well into the tail however these field lines are not open i.e. connected to IMF field. This region is adjacent to the region of the open field lines. From FAST data we find that the open field line boundary is usually at the poleward edge of the auroral oval beyond which polar rain is detected signifying open field lines connected to the IMF.

peak (a_1) for WIC represented by + and for SI-12 by asterisks. Prior to substorm onset the center of the Gaussian (a_1) of the electron auroras is slightly poleward of the proton auroras. There is a slight poleward motion of the auroral Gaussians in both plots. Immediately before onset there is a sudden equatorward movement of the WIC (+ signs) from 64 to 61 degrees. After onset there is a gradual poleward motion of the latitude of the Gaussian peak of the electrons and protons and they are seemingly moving together. The shape of the curves can be anticipated nicely from the keograms of Figure 11. At the end of the period the WIC seems to have moved greatly poleward in comparison with the protons. This is exaggerated by the fact that the Gaussian fit for the WIC latched on to the poleward branch (See Keogram Figure 11) while for the SI-12 it follows the equatorward branch. The latitude width parameter of the auroras was plotted in Figure 12d. In the pre-substorm phase we see some points that would represent extremely wide WIC auroras. These points represent the weak pre-substorm WIC auroras which are quite diffuse latitudinally. The relatively stronge pre-substorm proton band showed a considerably narrower region for the SI-12 data. It is interesting to note that the auroral oval narrowed just before onset. This is most likely to be caused by the auroral brightening of

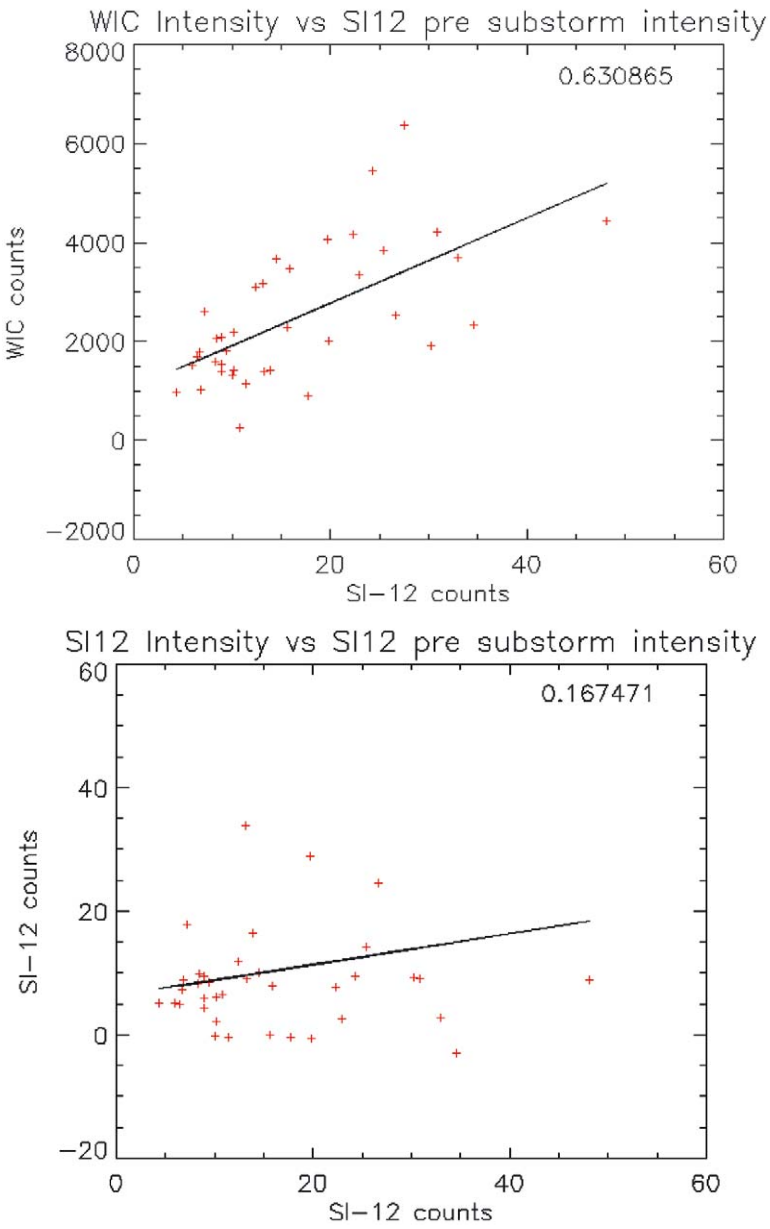

Figure 19. WIC intensity immediately after onset plotted against SI-12 intensity pre-onset (top, 19a). Both axes are instrument corrected counts. The correlation is 0.63, which is considerably higher than the correlation between SI-12 signal after onset vs. SI-12 signal before onset (bottom, 19b).

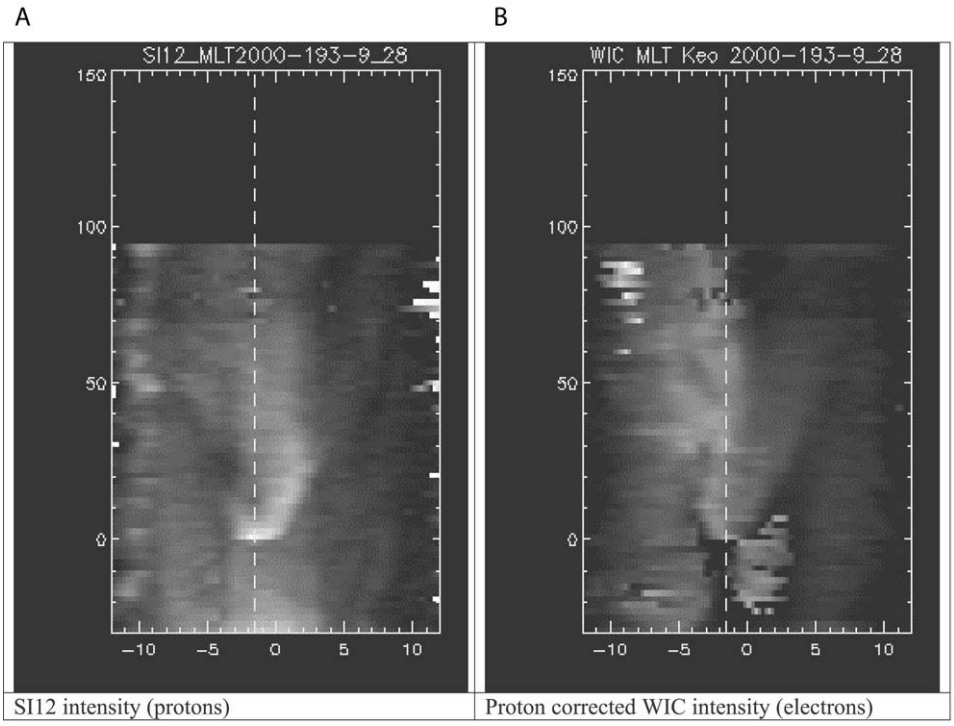

Figure 20. MLT Keogram where UT time (minutes) is going up and MLT is left (dusk) to right (dawn) in hours. Plot starts 30 min prior substorm onset. Figure 20a is for the SI-12 (protons) and Figure 20b is for WIC. The WIC signal was proton corrected so the intensity should represent pure electron precipitation.

the substorm arc feature, which is in fact best represented by an intense but narrow Gaussian form. At onset the oval widens which represent the well-known poleward expansion.

Having presented an individual case, we will now discuss the results in terms of the time history of the substorm parameters a_0, a_1 and a_2 for the entire set of substorms. Figure 13 shows the WIC intensity scatter plots with the mean of all the cases represented by a blue line. According to this data set the WIC intensity on average jumps from about 900 to 4000 AD units with a large scatter where the more intense substorms can reach as much as 8000-9000 WIC AD units. The average of the WIC intensity reaches its peak at about 5 min after onset after which it decays exponentially with a time constant of about 40 minutes. On figure14 we have plotted the SI-12 intensities. The SI-12 counts on average about double at substorm onset and has about the same decay as the WIC. The parameter a_1, representing the latitude of the Gaussian peak is plotted on Figure 15. The WIC data is shown in red while the SI-12 is in blue. The solid line represent the WIC average for all events and the broken line is the same for SI-12 average. It is important to note that the large scatter of the individual data points are partly caused by

the variation of the latitude of the substorm onset location. We have considered normalizing the latitude of the substorm onset location by shifting the latitude of each substorm to a common starting latitude. This would have been a similar procedure to normalization of the onset MLT. However it was thought that unlike MLT, the magnetic latitude is intrinsically non linear in magnetospheric space and one degree change in the magnetic latitude represents varying size regions in the magnetosphere and it would have been dangerous to normalize all substorms to the same onset latitude. Thus it should be recognized that the relative latitudinal motion of the fitted mean latitude parameter, a_1 represents the trends in the latitude motion of the aurora more accurately than the scatter of the data would suggest. Thus following interesting observations can be made: (1) The average of the WIC (electron) latitude mean is poleward of the protons prior to onset. (2) Just prior to onset the mean latitude of the peak WIC data proceeds rapidly equatorward until it is at the same latitude as the mean of the protons. (3) After the onset of the expansion phase the two WIC and SI-12 means are collocated while progressing gradually poleward. (4) The traces of the two averages track one-another for a whole hour after onset. In the later phases T+ 60 minutes the two separate and the WIC electrons take on their pre-substorm more poleward position. The next plot (Figure 16) is the latitude width parameter a_2 for WIC and SI-12. The same convention as with Figure 15 is followed. It should be noted that the SI12 resolution is about 1 degree from apogee and the WIC resolution is slightly better. In view of this our discussion is limited to auroral width of a degree or larger. Based mainly on the averages, represented by the solid (WIC) and broken (SI-12) lines, we can draw the following conclusions: (5) Pre-onset the proton aurora has a narrower latitude width than the electrons. (6) Just prior to onset the WIC auroras narrow drastically showing that the dominant intensity precipitation feature is quite narrow in latitude. (7) After onset both auroras widen in latitude with the protons apparently becoming the wider of the two. (8) After about 20 minutes or more the WIC electrons become the wider and this trend becomes more pronounced about one hour after onset.

5.0.1. *Discussion of the Superimposed Epoch analysis results*

The substorm onsets were identified with the temporal accuracy of the IMAGE satellite data, which is restricted by the two minute cadence. The intensity of the WIC data, representative of precipitating particle fluxes, on average jumped a factor of 5 from pre substorm to post substorm onset values. Newell *et al.* [2001] observed the pre-midnight total auroral power increase of a factor of 3.4. This seems to be inconsistent with our results because in addition to the increase of the peak intensity there is an increase in the area of the intense auroras, which would also contribute to the estimated total power. One possible cause of the discrepancy is that WIC detector includes a wider wavelength region than UVI and in these regions the auroral emissions are absorbed by O_2 between the aurora and the imager. *Newell et al.* [2001] analysis used only the high wavelength LBH detector which is more directly representative of the precipitating particle energy flux. If the substorm on-

set auroras had an intense component of low energy electrons then the discrepancy between the two studies could be consistent with this explanation. There is now evidence from IMAGE and FAST data that substorm onset aurora indeed contains large fluxes of low energy wave accelerated electrons [Mende *et al.*, 2003]. In our presentation we have not made the appropriate subtraction from the WIC data to remove the proton produced emissions. This left the data in a format that is better for comparisons with the UVI data.

The average intensity increase in the protons pre to post onset was about 2.2. Since there are no superimposed epoch analysis using proton auroral substorms we might try comparing our results with those of Birn *et al.* (1997) who also used the technique of superimposed epoch analysis of dispersionless injection of synchronous altitude particle data. Ion injections occur simultaneously with substorm onsets [e.g. Eather *et al.* 1976]. Birn *et al.* (1997) found minimal enhancement in the low energy ion component but the energetic ions (above 30 keV) contributed significantly and an average ion temperature enhancement from $\sim$10 to 16 keV was seen. These increases were assumed to come from an added new population. In summary the Birn *et al.* (1997) synchronous altitude satellite data does not show sufficient enhancement to account for our observed factor of two proton auroral intensification.

Our superimposed epoch analysis is consistent with many previous observations, which place the average of the electron precipitation to higher latitude than the mean of the protons prior to substorm onset. Just prior to onset the latitude of the mean representing the WIC data proceeds rapidly equatorward until it is at the same latitude as the mean of the protons. If we subscribe to the concept that the equatorward boundary of the proton aurora is the isotropic boundary [Sergeev *et al.*, 1993] then the peak of the electrons is located in the region of stretched but closed field lines. The peak of the electrons is also observed to narrow considerably prior to substorm onset however the sudden intensity of the break up auroras tend to have a narrow Gaussian latitude profile and it is possible that underlying weak auroras, which had been significant prior to onset, do not follow the same trends as the bright substorm arcs which tend to dominate our Gaussian fitting technique post onset. Otherwise the topological implications of this is that the onset occurs in the region of the proton precipitation that is in the region of closed field lines [Deehr *et al.*, 1994; Mende *et al.*, 2001] and by implication probably somewhat near the earth. After the onset in the initial minutes of the expansion phase the two WIC and SI-12 averages are collocated progressing gradually poleward. This is the same as was found earlier [Takahashi and Fukunishi, 2001; Mende *et al.*, 2001]. In our statistical analysis we found that the average traces of the protons and electrons track one-another for a whole hour after onset. This was not the case of the single substorm seen by Mende *et al.* (2001). We would expect that the two (electrons and protons) would separate in the later phases (T + 60 min) to take up their initial pre onset relative position. From Figure 16 depicting the latitude width parameter a_2 for WIC and SI-12 we notice that at pre-onset the proton aurora has

a narrower latitude width than the electrons. This is reasonably well known as the diffuse electron aurora usually spreads more poleward than the proton aurora. The narrowing of the WIC auroras just before onset was discussed above. After onset both auroras widen in latitude just as expected from the poleward expansion. There is also some evidence that the protons lead the expansion in the early phases. After about 20 minutes or more the WIC electrons become the wider of the two and this trend becomes more pronounced about one hour after onset. This is consistent with our expectations.

In Figure 17 we have plotted the mean position of the upper and lower Gaussian half height positions for the SI-12 in blue color while the upper terms one for WIC are in red. The low (or high) latitude half height positions were calculated by taking the mean latitude parameter, a_1 and subtracting (or adding) the width parameter, a_2 respectively. The parameter a_2 was normalized by multiplying it by 2.354/2 to represent the half width at half maximum height of a Gaussian.

As a summary we can discuss the mean Gaussian half height positions in relation to various boundaries of auroral/magnetospheric regions (Figure 18). The lowest boundary, represented in blue on Figure 17 is the mean equatorward half height boundary of the proton precipitation. This represents the boundary where we start seeing intense proton precipitation as we go to higher latitudes. In the magnetosphere proton precipitation starts at the isotropic boundary (IB) so named by Sergeev *et al.* (1993) where the trapped ring current pitch angle distribution is disturbed by the stretched field in the magnetic tail. Thus equatorward of the IB the curvature of the field is much less than the gyroradius of the protons and therefore the field does not significantly perturb the trapped proton distribution. The next, the poleward half height boundary is where the proton precipitation is reduced poleward (indicated in blue on Figure 17). There could be several causes for the existence of the poleward proton boundary. In the region 2, (Figure 18) equatorward of the boundary the field lines are definitely closed. The poleward boundary, where the precipitating proton intensity is reduced, does not have a clear definition. However it should be noted that the substorm onset is generally equatorward of this boundary.

It is very likely that the intensity of the auroral substorm after onset is proportional to the energy in the magnetosphere stored in the form of pre-onset plasma sheet population and tail stretching. If we assume that the intensity of the proton aurora pre-onset is a good representation of the near earth plasma sheet plasma density and the degree of tail stretching [Sergeev *et al.*, 1993] then we could expect that the intensity of the pre-onset proton aurora would correlate with the post onset intensity of the total (electron) precipitation. On Figure 19a we have produced a scatter plot of the post onset WIC intensity against the pre-onset SI-12 (proton) intensity. The plot indicates that such a trend might indeed exist. The cross correlation coefficient of 0.63 was found. As a comparison the SI12 intensity before and after onset show much poorer correlation with a coefficient of only 0.15 (Figure 19b).

5.0.2. *Magnetic Local Time Propagation*

It is relatively difficult to trace the motion of charged particle clouds in the magnetosphere as they drift in the non-uniform magnetic field and convect under the influence of electric fields. Considerable work has been done on tracing particles and electric fields from synchronous altitude satellite in situ particle detectors since the early work of DeForest and McIlwain (1971). If precipitating protons could be used as a footprint for plasma clouds then the azimuthal propagation of the proton auroras could be used to track magnetospheric energetic protons.

In the previous section we have introduced a technique of fitting a curve to the meridian profile of the auroras at various magnetic local times. Besides the removal of the dayglow this technique provided us with three characteristic parameters for the aurora at each magnetic local time region. The parameters were the peak intensity, a_0, the latitude of the peak, a_1, and the width of the aurora a_2. In Figure 20 we show a plot of the peak intensity parameter a_0 as a function of magnetic local time for one of the substorms (same substorm as Figure 11 and 12) included in our superposed epoch analysis. In the two-dimensional plot UT time is increasing upward and MLT is from left to right. Midnight is in the middle at MLT = 0. The afternoon dusk region therefore is left of the 0 MLT mark and dawn morning side is on the right. Time = 0 is the substorm onset time. Figure 20a is the SI-12 data showing the propagation of the proton aurora after substorm injection. The leading edge of the protons is moving towards the morning side. During the first 30 minutes the slope of the right edge of the proton trace is equivalent to a drift speed of 8 hours MLT drift per 1 hour UT. The surprise is not so much the size of the drift but rather its direction. It can be seen that the substorm injection occurred two hours pre-midnight but seemingly the proton aurora propagated towards the morning side contrary to the direction of gradient drift of energetic protons. If the protons were of very low energy then it is possible to expect an eastward drift under the influence of the electric field. In order to see the precipitating protons by the SI-12 instrument they must have initial proton energies greater than 1 keV at the top of the atmosphere.

Figure 20b shows WIC data for the same event using the same plotting technique described above for the SI-12 data. In this data the initial injection at T = 0 is quite symmetrical. It should be noted that in the WIC presentation the proton contribution was subtracted and we show only the residual luminosity, which is expected to be created by just the electrons. Since the electron precipitation is so dependent on the electric fields at relatively low altitudes we do not expect the WIC plots to be representative of magnetospheric particle drifts.

The dawnward propagation of the protons is somewhat unexpected as the gradient B drift carries energetic protons towards dusk. Schulz and Lanzerotti (1974) predict the particle drift speed as a function L value and particle energy. If the precipitating protons are of several keV energy, then the electric field which is needed to make them drift in the opposite (dawn) direction is quite substantial. In simulating the dispersionless substorm injections Li *et al.* (2000) propose an

inward propagating E-M field that would have a polarity such that in the temporary magnetic fields created by the E-M effect the ions would drift opposite to the quiescent earth magnetic fields. The proposed mechanism for these fields requires that the substorms start in the deep tail region and propagate towards the earth. As we have seen the location of the onset point in the bulk of the ion precipitation seem to indicate that the substorm onset is in the region of closed field lines near the boundary of dipole like and substantially distorted field lines. This highlights the most crucial yet still open question in magnetospheric physics regarding location of the substorm onset point in the magnetotail and the implication of that on substorm energization.

6. Conclusions

In this paper we review some of the highlights of the IMAGE FUV observations. Probably the most significant contribution of the IMAGE FUV system to satellite based auroral imaging is the new capability of making instantaneous global observations of proton precipitation through the detection of the Doppler shifted Lyman α emission. One great advantage of this observation technique is that the images are relatively free of dayglow contamination and that very clear pictures can be produced in all illumination conditions. This is an extremely powerful advantage for all auroral observations. Other than some low altitude satellite measurements, proton auroral measurements have been restricted to in situ particle or to ground based optical techniques. From the ground observation of the dayside proton aurora is seriously limited because of the faintness of Doppler shifted hydrogen emissions in the visible wavelength region. Therefore it is not surprising that some of the most significant IMAGE FUV observations were relevant to dayside proton auroral phenomena. For example IMAGE FUV was able to observe the dayside cusp in various conditions of IMF activity. In conditions of B_z positive the appearance of a distinct poleward auroral spot was reported, which correlates well with the predicted foot print of the cusp. The location of the spot is also in good agreement with the predicted location of the cusp based on theoretical considerations and the sense and magnitude of the B_y component. The intensity of the spot correlates well with the solar wind particle pressure. In summary all the observations are consistent with direct entry of a steady stream of solar wind particles through earth tail lobe field lines that are connected to the IMF. Even after the interaction of the solar wind with the bow shock and in the magnetosheath, the high-energy tail of the Maxwellian solar wind proton distribution has sufficient flux to account for our observations and no additional acceleration of the protons is necessary to produce the observed cusp optical emissions signatures. Occasionally low latitude dayside proton auroras are also observed in the noon-afternoon sectors and we find that in these instances protons are the primary component of the precipitating particle population. The three simultaneous emissions channel measurement of the IMAGE

FUV instrument and conjugate FAST in situ particle data showed that in this case the emission was entirely due to precipitating protons. These events are relatively rare, but often associated with high dynamic pressure in the solar wind and often seen to extend over more than 1 hour of local time. The mean energies observed by IMAGE and FAST are consistent with protons, which drift around the dusk sector after injection from the magnetotail near midnight

The high altitude global perspective permits the studying of substorms, unlike in situ satellite or ground based observations, which are greatly limited by the local time and latitude position of the observer. Based on the IMAGE FUV data from a single case substorm study it was concluded that in the pre-substorm phase at early evening local time the proton aurora was equatorward of the electron precipitation and near midnight they were collocated. The sudden brightening of the aurora at substorm onset near midnight was seen mostly in the electrons although there were protons present at this location. During the expansive phase both the electron and protons expanded poleward. The electron aurora formed a bright surge at the poleward boundary while the protons showed diffuse spreading. The presence of precipitating protons at the point where the initial brightening was seen showed that the substorm was initiated on closed field lines. In order to generalize these findings we have performed a superimposed epoch analysis of 59 substorms. To find suitable parameters that describe the latitude properties of the aurora and to eliminate the dayglow from the WIC images we fitted a Gaussian along the vertical (magnetic latitude axis) at each local time position. Since the spatial resolution of our global images was usually limited to about one degree of latitude a single Gaussian function described an equivalent aurora fairly well in most cases. The analysis of the mean of the gaussian parameters representing the latitude position of the gaussian peak showed that: (1) The mean of the WIC (electron) is poleward of the proton mean prior to onset. (2) Immediately prior to onset the mean the WIC data proceeds rapidly equatorward until it is at the same latitude as the mean of the protons. (3) After the onset of the expansion phase the two WIC and SI-12 means are collocated progressing gradually poleward. (4) The traces of the two means track one-another for a whole hour after onset. In the later phases (T+ 60 minutes) the two separate and the WIC electrons take on their pre-substorm, poleward position. Analysis of the parameter describing the width of the Gaussians showed that (5) Pre-onset the proton aurora has a narrower latitude width than the electrons. (6) Just prior to onset the WIC auroras narrow drastically. (7) Immediately after onset both auroras widen in latitude and the proton mean parameter becoming the wider of the two. (8) After about 20 minutes or more the WIC electrons become wider than the protons and this trend becomes more pronounced about one hour after onset. Analysis of the magnetic local time distribution of the auroras after substorm onset was also performed in a few cases. We used the peak intensity of the Gausian to represent the intensity at any local time. The results showed that the electrons spread similarly in the dawn dusk direction after onset. However the

protons have a distinct preference in propagating towards the dawn region after onset.

In conclusion this report is still about work which is very much in progress and we plan to perform more detailed in depth analysis about some of the topics mentioned and we are expecting to obtain several new results in the next few years.

Acknowledgements

We are grateful to the many people whose dedication and hard work resulted in the IMAGE FUV data set, this includes the NASA and South West Research Institute project team and the IMAGE-SMOC team. The IMAGE FUV investigation was supported by NASA through SWRI subcontract number 83820 at the University of California at Berkeley under contract number NAS5-96020. The solar wind measurements were obtained from CDAWeb. We acknowledge the following PIs: Wind Magnetic Fields Investigation: R. Lepping; Wind Solar Wind Experiment: K. Ogilvie; Geotail Magnetic Field Instrument: S. Kokubun; Geotail Comprehensive Plasma Instrument: L. Frank. J.-C. Gérard is supported by the Belgian National Fund for Scientific Research (FNRS). His work was funded by the PRODEX program of the European Space Agency (ESA) and the Belgian Fund for Collective Fundamental Research (grant FRFC 97-2.4569.97). We are indebted to the PI C.W. Carlson for use of FAST data.

References

Anderson, B.J. and Hamilton, D.C.: 1993, 'Electromagnetic ion cyclotron waves stimulated by modest magnetospheric compressions', *J. Geophys. Res.* **98**, 11369–11382.

Anger, C.D., Moshupi, M.C., Wallis, D.D., Murphree, J.S., Brace, L.H. and Shepherd, G.G.: 1979, 'Detached auroral arcs in the trough region', *J. Geophys Res.* **84**, 1333–1346.

Anger, C.D., Babey, S.K., Lyle Broadfoot, A., Brown, R.G., Cogger, L.L., Gattinger, R., Haslett, J.W., King, R.A., McEwen, D.J., Murphree, J.S., Richardson, E.H., Sandel, B.R., Smith, K. and Jones, A.V.: 1987, 'An ultraviolet auroral imager for the Viking spacecraft', *Geophys. Res. Lett.* **14**, 387.

Birn, J., Thomsen, M.F., Borovsky, J.E., Reeves, G.D., McComas, D.J. and Belian, R.D.: 1997, 'Characteristic plasma properties during dispersionless substorm injections at geosynchronous orbit', *J. Geophys. Res.*, **102**, 2309–24.

Brice, N. and Lucas, C.: 1975, 'Interaction between heavier ions and ring current protons', *J. Geophys. Res.* **80**, 936–942.

Burch, J.L.: 1968, 'Low-energy electron fluxes at latitudes above the auroral zone', *J. Geophys. Res.* **73**, 3585.

Burch, J.L.: 2000, 'Image mission overview', *Space Sci. Rev.* **91**, 1–14.

Burch J.L., Lewis, W.S., Immel, T.J., Anderson, P.C., Frey, H.U., Fuselier, S.A., Gerard, J.-C., Mende, S.B., Mitchell, D.G. and Thomsen, M.F.: 2002, 'Interplanetary magnetic field control of afternoon-sector detached proton arcs', *J. Geophys. Res.* **107**(A9), 1251, doi:1029/2001JA007554.

Cann, M.N., McPherron, R.L. and Russell, C.T.: 1975, 'Substorm and interplanetary magnetic field effects on the geomagnetic tail lobes', *J. Geophys. Res.* **80**, 191-4.

Carlson, C.W., McFadden, J.P., Turin, P., Curtis, D.W. and Magoncelli, A.: 2001, 'The electron and ion plasma experiments for FAST', *Space Sci. Rev.* in press.

Chang, S.-W., Mende, S.B., Frey, H.U., Gallagher, D.L. and Lepping, R.P.: 2002, 'Proton aurora dynamics in response to the IMF and solar wind variations', *Geophys. Res. Lett.* **29**, 10.1029/2002GL015019.

Deehr, C.S.: 1994, 'Ground based optical observations of hydrogen emissions in the auroral substorm', Proceedings of the International Conference on Substorms 2, Fairbanks, USA. P229-236.

DeForest, S.E. and McIlwain, C.E.: 1971, 'Plasma clouds in the magnetosphere', *J. Geophys. Res.*, **76**, 3587–3611.

Dunlop, M.W., Cargill, P.J., Stubbs, T.J. and Woolliams, P.: 2000, 'The high-altitude cusps: HEOS2', *J. Geophys. Res.* **105**, 27509.

Eather, R.H.: 1967, 'Auroral proton precipitation and hydrogen emissions', *Rev. Geophys.* **5**, 207–285.

Eather, R.H., Mende, S.B. and Judge, R.J.R.: 1976, 'Plasma injection at synchronous orbit and spatial temporal auroral morphology', *J. Geophys. Res.* **81**, 2805, 1976.

Elphinstone, R.D., Murphree, J.S. and Cogger, L.L.: 1996, 'What is a global auroral substorm?' *Rev. Geophys.* **34**, 169–232.

Frank, L.A.: 1971, 'Plasma in the earth's polar magnetosphere', *J. Geophys. Res.* **76**, 5202–19.

Frank, L.A., Craven, J.D., Ackerson, K.L., English, M.R., Eather, R.H. and Crovillano, R.L.: 1981, 'Global auroral imaging instrumentation for the Dynamics Explorer mission', *Space Sci. Instrum.* **5**, 369–393.

Frank, L.A. and Craven, J.D.: 1988, 'Imaging results from Dynamics Explorer 1', *Rev. Geophys.* **2**, 249.

Frey, H.U., Mende, S.B., Carlson, C.W., Gérard, J.-C., Hubert, B., Spann, J., Gladstone, R. and Immel, T.J.: 2001, 'The electron and proton aurora as seen by IMAGE-FUV and FAST', *Geophys. Res. Lett.* **28**, 1135.

Frey, H.U., Mende, S.B., Immel, T.J., Fuselier, S.A., Claflin, E.S., Gérard, J.-C. and Hubert, B.: 2002, 'Proton aurora in the cusp', *J. Geophys. Res.* **107**, (A7), 1091, 10.1029/2001JA900161.

Frey, H.U., Mende, S.B., Immel, T.J., Gérard, J.-C., Hubert, B., Habraken, S., Spann, J. and Gladstone, R.: 2003, 'Summary of quantitative interpretation of image far ultraviolet auroral data', *Space Sci. Rev.* this issue.

Fukunishi, H.: 1975, 'Dynamic relationship between proton and electron auroral substorms', *J. Geophys. Res.* **80**, 533.

Fuselier, S.A., Anderson, B.J. and Onsager, T.G.: 1997, 'Electron and ion signatures of field line topology at the low-shear magnetopause', *J. Geophys. Res.* **102**, 4847.

Fuselier, S.A., Ghielmetti, A.G., Moore, T.E., Collier, M.R., Quinn, J.M., Wilson, G.R., Wurz, P., Mende, S.B., Frey, H.U., Jamar, C., Gérard, J.-C. and Burch, J.L.: 2001, 'Ion outflow observed by IMAGE: Implications for source regions and heating mechanisms', *Geophys. Res. Lett.* **28**, 1163.

Fuselier, S.A., Frey, H.U., Trattner, K.J., Mende, S.B. and Burch, J.L.: 2002, 'Cusp aurora dependence on IMF B_Z', *J. Geophys. Res.* **107**, (A7), 1029/2002JA900165.

Gérard, J.-C., Hubert, B., Bisikalo, D.V. and Shematovich, V.I.: 2000, 'A model of the Lyman-α line profile in the proton aurora', *J. Geophys. Res.* **105**, 15795.

Gérard, J.-C., Hubert, B., Bisikalo, D.V., Shematovich, V.I., Frey, H.U., Mende, S.B., Meurant, M., Gladstone, G.R. and Carlson, C.W.: 2001, 'Observation of the proton aurora with IMAGE-FUV and simultaneous ion flux in situ measurements', *J. Geophys. Res.* **106**, 28939.

Germany, G.A., Parks, G.K., Brittnacher, M., Cumnock, J., Lummerzheim, D., Spann, J.F., Chen, L., Richards, P.G. and Rich, F.J.: 1997, 'Remote determination of auroral energy characteristics during substorm activity', *Geophys. Res. Lett.* **24**, 995–998.

Gorney, D.J. and Evans, D.S.: 1987, 'The low-latitude auroral boundary: steady state and time-dependent representations', *J. Geophys. Res.* **92**, 13537-45.

Hardy, D.A., Gussenhoven, M.S. and Holeman, E.: 1985, 'A statistical model of auroral electron precipitation', *J. Geophys. Res.* **90**, 4229.

Hardy, D.A., Gussenhoven, M.S., Raistrick, R. and McNeil, W.J.: 1987, 'Statistical and functional representations of the pattern of auroral energy flux, number flux, and conductivity', *J. Geophys. Res.* **92**, 12275–12294.

Hardy, D.A., Gussenhoven, M.S. and Brautigam, D.: 1989, 'A statistical model of auroral ion precipitation', *J. Geophys. Res.* **94**, 370.

Hardy, D.A., McNeil, W., Gussenhoven, M.S. and Brautigam, D.: 1991, A statistical model of auroral ion precipitation, 2. Functional representation of the average patterns, *J. Geophys. Res.* **96**, 5539.

Hecht, J.H., McKenzie, D.L., Christensen, A.B., Strickland, D.J., Thayer, J.P. and Watermann, J.: 2000, 'Simultaneous observations of lower thermospheric composition change during moderate auroral activity from Kangerlussuaq and Narsarsuaq, Greenland', *J. Geophys. Res.* **105**, 27109–27118.

Heikkila, W.J. and Winningham, J.D.: 1971, 'Penetration of magnetosheath plasma to low altitudes through the dayside magnetospheric cusps', *J. Geophys. Res.* **76**, 883–891.

Hubert, B., Gérard, J.-C., Bisikalo, D.V. and Shematovich, V.I. and Solomon, S.C.: 2001, 'The role of proton precipitation in the excitation of the auroral FUV emissions', *J. Geophys. Res.* **106**, 21,475–21,494.

Hubert, B, Gérard, J.-C., Evans, D.S., Meurant, M., Mende, S.B., Frey, H.U. and Immel, T.J.: 2002, 'Total electron and proton energy input during auroral substorms: Remote sensing with IMAGE-FUV', *J. Geophys. Res.* **107**, (A8), 10.1029/2001JA009229.

Immel, T.J., Craven, J.D. and Nicholas, A.C.: 2000, 'An empirical model of the OI FUV dayglow from DE-1 images', *J. Atmos. and Solar-Terr. Phys.* **62**, 47–64.

Immel, T.J., Mende, S.B., Frey, H.U., Peticolas, L.M. and Carlson, C.W.: 2002, 'Precipitation of auroral protons in detached arcs', *Geophys. Res. Lett.* **29**(11), 10.1029/2001GL013847.

Ishimoto, M., Meng, C.-I., Romick, G.R. and Huffman, R.E.: 1989, 'Doppler shift of auroral Lyman a observed from a satellite', *Geophys. Res., Lett.* **16**, 117–218.

Jordanova, V.K., Farrugia, C.J., Thorne, R.M., Khazanov, G.V., Reeves, G.D., Thomsen, M.F.: 2001, 'Modeling ring current proton precipitation by electromagnetic ion cyclotron waves during the May 14-16, 1997, storm', *J. Geophys. Res.* **106**, 7–22.

Li, X., Baker, D.N., Temerin, M., Peterson, W.K. and Fennell, J.F.: 2000, 'Multiple discrete-energy ion features in the inner magnetosphere: observations and simulations', *Geophys. Res. Lett.* **27**, 1447–1450.

Lyons, L.R. and Samson, J.C.: 1992, 'Formation of the stable arc that intensifies at substorm onset', *Geophys. Res. Lett.* **19**, 2171–2174.

Mende, S.B. and Eather, R.H.: 1976, 'Monochromatic all sky observations and auroral precipitation patterns', *J. Geophys. Res.* **81**, 3771–3780.

Mende, S.B. et al.: 2000, 'Far ultraviolet imaging from the IMAGE spacecraft. 3. Spectral imaging of Lyman- alpha and O I 135.6 nm', *Space Sci. Rev.* **91**, 287–318.

Mende, S.B., Frey, H.U., Lampton, M., Gèrard, J.-C., Hubert, B., Fuselier, S., Spann, J., Gladstone, R. and Burch, J.L.: 2001, 'Global observations of proton and electron auroras in a substorm', *Geophys. Res. Lett.* **28**, 1139.

Mende, S.B., Frey, H.U., Carlson, C.W., McFadden, J., Gerard, J.-C., Hubert, B., Fuselier, S.A., Gldstone, G.R. and Burch, J.L.: 2002, 'IMAGE and FAST observations of substrom recovery phase aurora', *Geophys. Res. Lett.* **29**, 10.1029/2001GL013027.

Mende, S.B., Carlson, C.W., Frey, H.U., Immel, T.J. and Gérard, J.-C.: 2003, 'IMAGE FUV and in situ FAST particle observations of substorm aurorae', *J. Geophys. Res.* **108**(A4), 8010, doi: 10.1029/2002JA009413.

Milan, S.E., Lester, M., Cowley, S.W.H. and Brittnacher, M.: 2000, 'Dayside convection and auroral morphology during an interval of northward interplanetary magnetic field', *Ann. Geophys.* **18**, 436–444.

Montbriand, L.E.: 1971, 'The proton aurora and auroral substorm', in *Radiating Atmosphere*, *in* B.M. McCormac and D. Reidel (eds), Hingham, Mass, p. 366.

Moshupi, M.C., Anger, C.D., Murphree, J.S., Wallis, D.D., Whitteker, J.H. and Brace, L.H.: 1979, 'Characteristics of trough region auroral patches and detached arcs observed by ISIS 2', *J. Geophys Res.* **84**, 1333–1346.

Murphree, J.S., King, R.A., Payne, T., Smith, K., Reid, D., Adema, J., Gordon, B. and Wlochowicz, R.: 1994, 'The Freja Ultraviolet Imager', *Space Sci. Rev.* **70**, 421–446.

Newell, P.T., Meng, C.-I., Sibeck, D.G. and Lepping, R.: 1989, 'Some low-altitude cusp dependencies on the interplanetary magnetic field', *J. Geophys. Res.* **94**, 8921-8927.

Newell, P.T. and Meng, C.I.: 1994, 'Ionospheric projections of magnetospheric regions under low and high solar wind pressure conditions', *J. Geophys. Res.* **99**, 273.

Newell P.T, Feldstein, Y.I., Galperin, Y.I. and Meng, Ching-I: 1996, 'Morphology of nightside precipitation', *J. Geophys. Res.* **101**, 10737–10748.

Newell, P.T., Liou, K., Sotirelis, T. and Meng, C.I.: 2001, 'Auroral precipitation power during substorms: a POLAR UV imager-based superposed epoch analysis', *J. Geophys. Res.* **106**, 28885–28896.

Nilsson, H., Kirkwood, S. and Moretto, T.: 1998, 'Incoherent scatter radar observations of the cusp acceleration region and cusp field-aligned currents', *J. Geophys. Res.* **103**, 26721.

Øieroset, M., Sandholt, P.E., Denig, W.F. and Cowley, S.W.H.: 1997, 'Northward interplanetary magnetic field cusp aurora and high-latitude magnetopause reconnection', *J. Geophys. Res.* **102**, 11349, 1997.

Onsager, T.G. and Fuselier, S.A.: 1994, 'The location of magnetic reconnection for northward and southward interplanetary magnetic field', *in* J.L. Burch and J.H. Waite *Solar System Plasmas in Space and Time*, p. 183.

Reiff, P.H., Hill, T.W. and Burch, J.L.: 1977, Solar wind plasma injection at the dayside magnetospheric cusp, *J. Geophys. Res.* **82**, 479.

Reiff, P.H. and Burch, J.L.: 1985, 'IMF B_Y-dependent plasma flow and Birkeland currents in the dayside magnetosphere, II'. A global model for northward and southward IMF, *J. Geophys. Res.* **90**, 1595.

Rostoker, G., Spadinger, I. and Samson, J.C.: 1984, Local time variation in the response of Pc 5 pulsations in the morning sector to substorm expansive phase onsets near midnight, *J. Geophys. Res.* **89**, 6749–6757.

Russell, C.T., Montgomery, M.D., Neugebauer, M., Scarf, F.L. and Chappell, C.R.: 1971, 'Ogo 5 observations of the polar cusp on November 1, 1968', *J. Geophys. Res.*, **76**, 6743–6764.

Samson, J.C. and Yeung, K.L.: 1986, 'Some generalizations on the method of superposed epoch analysis', *Planetary and Space Science* **34**, 1133–1142.

Samson, J.C., Lyon, L.R., Newell, P.T., Creutzberg, F. and Xu, B.: 1992, 'Proton aurora and substorm intensification', *Geophys. Res. Lett.* **19**, 2167.

Sandel, B.R, King, R.A., Forrester, W.T., Gallagher, D.L., Broadfoot, A.L. and Curtis, C.C.: 2001, 'Initial results from the IMAGE Extreme Ultraviolet Imager', *Geophys. Res. Lett.* **28**, 1439–1442.

Sandholt, P.E.: 1997, 'Dayside polar cusp/cleft aurora: morphology and dynamics', *Phys. Chem. Earth* **22**, 675.

Sandholt, P.E., Farrugia, C.J., Moen, J., Noraberg, O., Lybekk, B., Sten, T. and Hansen, T.: 1998, 'A classification of dayside auroral forms and activities as a function of interplanetary magnetic field orientation', *J. Geophys. Res.* **103**, 23325.

Schultz, M., Lanzerotti, L.J.: 1974, 'Particle diffusion in the radiation belts', Berlin, West Germany: Springer-Verlag, ix+215 pp.

Sergeev, V.A. and Malkov, M.V.: 1988, 'Diagnostic of energetic electrons above the ionosphere', *Geoman. Aeron.* **28**, 549.

Sergeev, V.A., Malkov, M. and Mursula, K.: 1993, 'Testing the isotrop boundary algorithm method to evaluate the magnetic field configuration', *J. Geophys. Res.* **98**, 7609–7620.

Siscoe, G.L.: 1991, 'What determines the size of the auroral oval, in Auroral Physics', *in* C.-I. Meng, M.J. Rycroft and L.A. Frank, Cambridge University Press, New York, p. 159.

Smith, M.F. and Lockwood, M.: 1996, Earth's magnetospheric cusps, *Rev. Geophys.* **34**, 233.

Takahashi, Y. and Fukunishi, H.: 2001, 'The dynamics of the proton aurora in auroral break up events', *J. Geophys. Res.* **106**, 45–64.

Torr, M.R. et al.: 1995, 'A far ultraviolet imager for the international solar-terrestrial physics mission', *Space Sci. Rev.* **71**, 329.

Tsyganenko, N.A.: 1990, 'Quantitative models of the magnetospheric magnetic field: methods and results', *Space Sci. Rev.* **54**, 75–186.

Vallance-Jones, A., Creutzberg, F., Gattinger, R.L., Harris, F.A.: 1982, 'Auroral studies with a chain of meridian scanning photometers 1'. Observations of proton and electron aurora in magnetospheric substorms, *J. Geophys. Res.* **87**, 4489.

Vo, H.B. and Murphree, J.S.: 1995, 'A study of dayside auroral bright spots seen by the Viking auroral imager', *J. Geophys. Res.* **100**, 3649–3655.

Walker, R.J. and Russell, C.T.: 1995, 'Solar-wind interactions with magnetized planets', *in* M.G. Kivelson and C.T. Russell (eds), *Introduction to Space Physics*, Cambridge Univ. Press, Cambridge, p. 178.

Woch, J. and Lundin, R.: 1992, 'Magnetosheath plasma precipitation in the polar cusp and its control by the interplanetary magnetic field', *J. Geophys. Res.* **97**, 1421.

Yamauchi, M. and Lundin, R.: 2001, 'Comparison of various cusp models with high- and low-resolution observations', *Space Sci. Rev.* **95**, 457.

Zhang, Y., Paxton, L., Immel, T.J., Frey, H.U. and Mende, S.B.: 2003, 'Sudden solar wind dynamic pressure enhancements and dayside detached aurora: IMAGE and DMSP observations', *J. Geophys. Res.* **108**, (A4) 8001,doi:10.1029/2002JA009355.

Zhou, Xiaoyan and Tsurutani, B.T.: 1999, 'Rapid intensification and propagation of the dayside aurora: large scale interplanetary pressure pulses (fast shocks)', *Geophys. Res. Lett.* **26**, 1097–100.

Zwick, H.H. and Shepherd, G.G.: 1963, 'Some observations of hydrogen line profiles in the aurora', *J. Atmospheri Terrest. Phys.* **25**, 604–607.